Van der Waals Heterostructures

Andres Castellanos-Gomez,[1] Xiangfeng Duan,[2,3] Zhe Fei,[4,5] Humberto Rodriguez Gutierrez,[6] Yuan Huang,[7] Xinyu Huang,[7]Jorge Quereda,[8] Qi Qian,[2] Eli Sutter,[9,10] and Peter Sutter[11,*]

[1]Materials Science Factory, Instituto de Ciencia de Materiales de Madrid (ICMM-CSIC), Madrid, Spain
[2]Department of Chemistry and Biochemistry, University of California Los Angeles, Los Angeles, CA 90095, USA
[3]California NanoSystems Institute, University of California Los Angeles, Los Angeles, CA 90095, USA
[4]Department of Physics and Astronomy, Iowa State University, Ames, IA 50011, United States
[5]Ames Laboratory, U.S. Department of Energy, Iowa State University, Ames, IA 50011, United States
[6]Department of Physics, University of South Florida, Tampa, FL 33620, USA
[7]Advanced Research Institute of Multidisciplinary Science, Beijing Institute of Technology, Beijing, China
[8]GISC, Departamento de Física de Materiales, Universidad Complutense de Madrid, Madrid, Spain
[9]Department of Mechanical and Materials Engineering, University of Nebraska-Lincoln, Lincoln, NE 68588, USA
[10]Nebraska Center for Materials and Nanoscience, University of Nebraska-Lincoln, Lincoln, NE 68588, USA
[11]Department of Electrical and Computer Engineering, University of Nebraska-Lincoln, Lincoln, NE 68588, USA

[*]Email: psutter@unl.edu

Abstract

The integration of dissimilar materials into heterostructures has become a powerful tool for engineering interfaces and electronic structure. The advent of two-dimensional (2D) materials brought unprecedented opportunities for novel heterostructures in the form of van der Waals stacks, laterally stitched 2D layers, and more complex layered and 3D architectures. This Primer provides an overview of state-of-the-art methodologies for producing such van der Waals heterostructures, focusing on the two fundamentally different strategies, top-down deterministic assembly and bottom-up synthesis. For both approaches, successful techniques, advantages, and limitations are discussed. As important as the fabrication itself is the characterization of the resulting engineered materials, for which a range of analysis techniques covering structure, composition, and emerging functionality are highlighted. Examples of the properties of artificial van der Waals structures include optoelectronics and plasmonics, twistronics, and unique functionality arising from the generalization of van der Waals assembly from 2D- to 3D-crystalline components. Finally, current issues of reproducibility, limitations, and opportunities for future breakthroughs in terms of enhanced homogeneity, interfacial purity, feature control, and ultimately orders of magnitude increased complexity of van der Waals heterostructures are discussed.

Introduction

Materials integration in heterostructures is a mainstay of modern materials science, enabling applications such as semiconductor lasers,[1,2] light emitting diodes[3] and fast transistors[4]. New functionality can originate from the interface between dissimilar materials,[5,6] or from the stacking of crystals with different electronic structure, creating **quantum wells**, superlattices or other potential energy landscapes that modify or confine carrier wavefunctions.[7]

Epitaxial heterostructures of three-dimensional (3D) crystals such as silicon, germanium, or gallium arsenide are subject to stringent compatibility requirements, where the components need to have the same crystal structure to allow for epitaxy,[8] and their lattice constants should not differ by more than a few percent. Even systems with moderate lattice mismatch, such as germanium/silicon (Figure 1a), allow pseudomorphic strained-layer growth only for a limited thickness,[9] followed by strain relaxation mechanisms that progress from surface roughening[10] to eventual plastic deformation by introduction of misfit dislocations.[11]

The advent of van der Waals epitaxy,[12] and especially the ability to isolate and manipulate two-dimensional (2D) materials[13] opened up vast opportunities for materials integration in heterostructures.[14,15] Through stacking of 2D layers without covalent bonds but only weak dispersion forces at the interfaces (Figure 1b), dissimilar materials can be combined into heterostructures without any of the limitations that apply in epitaxy. The individual layers can have different crystal symmetry, structure, and lattice parameters. Even the orientation can be varied, giving rise to new degrees of freedom such as interlayer twist.[16] In fact, the components of such stacks can even comprise 3D crystals, provided that their surfaces are properly terminated to limit the interfacial interaction to van der Waals forces.

In addition to vertical van der Waals stacks, atomically thin 2D crystals can be integrated into lateral heterostructures (Figure 1b).[17,18] While not strictly considered as van der Waals heterostructures, such heterogeneous 2D membranes pursue the same goal, namely the creation of interfaces where new phenomena arise from joining components with different electronic structure. In contrast to vertical stacks, which can be fabricated either by **exfoliation** and **micromechanical assembly** or van der Waals epitaxy, lateral heterostructures are accessible only by bottom-up synthesis and are subject to some of the compatibility criteria that apply to 3D crystals.

In this Primer, contemporary methodologies for creating van der Waals heterostructures are reviewed. Advanced techniques for exfoliating large-area 2D crystals are discussed, followed by an account of micromechanical stacking of such atomically thin flakes, which can be generalized to include 3D crystals as building blocks. Mechanical assembly is contrasted by bottom-up synthesis approaches for both vertical and lateral heterostructures, as well as architectures that go beyond the two archetypes to form more complex interface geometries. The fabrication of twisted homostacks and heterostacks, structures of intense interest, almost exclusively involves mechanical assembly. There is a clear need for synthesis methods capable of creating twisted interfaces; some of the promising approaches developed so far are discussed. Given that they extend from the atomic to macroscopic scales, characterizing van der Waals heterostructures poses significant challenges. Following a discussion of experimental methods for assessing structure, composition, and key properties, the versatility of van der Waals heterostructures is

demonstrated by highlighting examples of their emerging properties. Finally, issues of reproducibility, current limitations, as well as future opportunities for continued development of van der Waals heterostructures are discussed.

Experimentation

With few exceptions of naturally occurring materials, van der Waals heterostructures are human-made, artificial structures that can be fabricated either by top-down or bottom-up processes. In this section, the different fabrication processes for van der Waals heterostructures are discussed. Top-down approaches involve the mechanical stacking of 2D crystals, often isolated from bulk layered materials by exfoliation. Bottom-up fabrication is based on crystal growth processes, where consecutive components are added by supplying suitable, often gas phase or vapor phase, precursors at high temperatures. As an alternative, spontaneous processes such as phase separation can be harnessed to create unconventional heterostructures that are not simply vertical stacks or laterally stitched membranes.

Mechanical stacking

Large-scale 2D crystal exfoliation

Exfoliation from bulk crystals is one of the most important approaches for producing 2D materials for assembly into van der Waals heterostructures. Since the first isolation of graphene, mechanical exfoliation has been widely used for preparing 2D crystals.[13,19-22] The high quality of these exfoliated materials has allowed their intrinsic properties to be studied. However, the simple scotch tape exfoliation method faces serious limitations, mainly a low yield and limited flake size.

The quest for large-area 2D materials involves two opposing philosophies. Bottom-up strategies such as chemical vapor deposition (CVD) can produce uniform materials at wafer scale and are therefore considered superior in obtaining large-area 2D crystals, but they often involve strong coupling to the substrate[23-26] that may affect the physical properties and complicate isolation and transfer. Nevertheless, bottom-up synthesis followed by mechanical transfer promises to become an important technology for fabricating stacked van der Waals heterostructures at large scales. The alternative approach entails the optimization of top-down exfoliation to obtain large-area 2D crystals. To achieve this goal, the relevant interfacial interactions need to be considered. The van der Waals force is the primary interlayer interaction in most layered bulk crystals and the interfacial interaction with a substrate. It depends on two key parameters: the contact distance and the dipole moment of the atoms. Monolayer flakes can be exfoliated from a layered bulk crystal if the interaction between the substrate and the outermost layer exceeds the interlayer interaction in the crystal. Therefore, to enhance the exfoliation yield there is a need to find ways of reducing the separation from the substrate and increasing the dipolar interaction.

Most exfoliation is carried out in air and so the presence of adsorbed molecules on the surfaces is unavoidable. Molecules trapped between a layered crystal and a substrate increase the separation and screen (weaken) the dipolar interaction. This issue is successfully addressed in an oxygen plasma enhanced exfoliation method, where removal of adsorbed molecules from the SiO_2/silicon substrate reduces the contact distance, yielding flakes of graphene and of the high-temperature superconductor bismuth-2212 at millimeter scale.[27,28]

Unlike graphene, the unit cell of most 2D crystals contains several atomic layers. Each MoS_2 unit, for example, involves a sulphur-molybdenum-sulphur trilayer. In such cases, the interaction

with a substrate is mostly governed by the surface atoms. Oxygen plasma enhanced exfoliation does not readily yield large-area MoS_2 since the dipolar interaction between sulphur in MoS_2 and oxygen in SiO_2 is weak. Several groups have tried different ways to optimize mechanical exfoliation, for example, using gold films to exfoliate MoS_2 and other transition metal dichalcogenides (TMDs).[29-31] Al_2O_3 was also used to exfoliate 2D materials, facilitating the fabrication of electronic devices,[32] but the exfoliation mechanism is not well understood. A universal exfoliation method using ultrathin gold adhesion layers was reported to have successfully prepared 40 kinds of 2D materials at macroscopic scale (Figure 2).[33] The unifying concept, confirmed by calculations, is that most layered crystals interact strongly with gold, especially those whose surface layer contains main group (group V, VI, VII) non-metals. These elements engage in covalent-like quasi-bonding with gold, which tends to be stronger than the interlayer interaction in the source crystal. New developments, such as gold-assisted exfoliation, for producing 2D materials with millimeter to centimeter size satisfy the demand for high-quality monolayer crystals, including suspended 2D materials,[34] and also supply the toolkit for fabricating a myriad of van der Waals heterostructures by transfer and mechanical stacking.[35]

Assembly of van der Waals stacks

The past decade has seen rapid advances in the approaches for mechanically stacking 2D materials to form van der Waals heterostructures.[36] Current techniques allow picking up arbitrary 2D materials and stacking them with great control over their position and relative orientation, regardless of their lattice parameters. This is achieved by using dedicated systems which typically rely on the use of an optical microscope, three-axis micropositioners, and rotational stages to achieve sub-micrometer precision in the lateral positioning of the transferred flakes and rotation precision of less than 1° when stacking layers with a user defined twist angle.[37,38] Note that while most of these setups are manually operated under ordinary atmospheric conditions, an increasing number of systems are being installed in gloveboxes or even vacuum chambers, using motorized stages, to gain more control over the environmental conditions, reduce contamination and enhance the reproducibility of the transfer processes. The most common transfer methods can be divided into two main categories: wet and dry transfer techniques, depending on whether they rely on the use of soluble sacrificial layers.

The basis for wet-transfer techniques using water-soluble layers was developed in 2010.[39] Figure 3a shows schematically the main steps. First, a SiO_2/silicon substrate is **spin-coated** with a water-soluble polymer, followed by a layer of poly(methyl methacrylate) (PMMA). Atomically thin flakes are then exfoliated onto the polymer sheet. Upon immersion in water the soluble layer is removed, leaving the PMMA layer carrying the flakes floating on the water, from where it can be picked up with a glass slide. Finally, the PMMA is placed flake-down onto a target flake with the help of a three-axis micromanipulator, followed by the removal of the PMMA by immersion in acetone to obtain the final heterostructure. Later variants of this wet-transfer eliminated the water solvents and instead relied on mechanically peeling off the PMMA from the SiO_2 substrate using an adhesive tape, thus making the process less susceptible to contamination.[40]

Wet transfer techniques require dissolving sacrificial polymer layers on top of the 2D crystals, which tends to introduce wrinkles in the resulting heterostructures and results in the adsorption of molecules on the crystal surface, ultimately requiring the use of organic solvents to remove these residues. Dry-transfer methods,[41] on the other hand, avoid sacrificial polymers and instead use a viscoelastic polymer such as polydimethylsiloxane (PDMS) to pick up and release 2D

crystals. The main steps of this transfer method are depicted in Figure 3b. First, atomically thin crystals are exfoliated and identified on a SiO_2/silicon substrate. Then, a PDMS stamp is placed on top of the substrate. Due to its viscoelastic nature, PDMS can slowly deform, conforming to the surface of the underlying substrate and flakes to form an intimate contact and adhere to the crystals. The flakes are picked up by rapidly separating the stamp from the SiO_2/silicon substrate. The stamp can later be positioned on top of a target flake, brought into contact, and slowly peeled off to release the attached crystals and create a van der Waals stack. An alternative dry-transfer approach relies on the use of vitreous polymers, such as polypropylene carbonate (PPC), polycarbonate, or nitrocellulose, whose adhesion strength can be adjusted by tuning the temperature to values close to their melting point (around 170°C for PPC, 150°C for polycarbonate, and about 100°C for nitrocellulose).[42]

While dry-transfer techniques largely reduce the degradation of van der Waals stacks due to mechanical deformation and adsorption of molecules, they still bring the crystals in contact with polymers. To further improve sample quality, several groups have recently developed an alternative assembly technique for van der Waals heterostructures sandwiched between hexagonal boron nitride (h-BN) flakes.[42] The process, shown in Figure 3c, starts by exfoliating h-BN onto SiO_2 and picking up a flake using a PPC stamp. The h-BN supported by the polymer stamp is then placed on top of another few-layer crystal, which is picked up by van der Waals interaction with the h-BN surface. This process can be repeated to pick up additional layers. Finally, the complete heterostructure is placed onto a substrate and the PPC is melted and removed by organic solvents. The main advantage of the h-BN pickup method is that the inner layers of the heterostructure are never in contact with polymers or solvents, resulting in extremely clean and homogeneous interfaces. This, however, comes at the price of increased complexity and reduced fabrication yield compared to the simpler PDMS based dry-transfer.

Bottom-up synthesis

Vertical and lateral heterostructures

Vertical van der Waals heterostructures can be fabricated either by exfoliation and stacking or van der Waals epitaxy, whereas lateral heterostructures can be realized only via synthesis. Two different methodologies can be distinguished. In pure bottom-up approaches, a heterostructure is formed by edge-epitaxy of the different constituent materials.[43-53] Combined top-down/bottom-up methods involve patterning of 2D crystals by lithography,[54,55] focused ion beam etching,[56] or laser writing,[57,58] followed by growth[56] or chalcogen exchange.[54,55]

One of the most popular methods to produce 2D materials is CVD, due to its simplicity and material flexibility. With minor variations, CVD systems[59] consist of four basic components: A gas delivery system that controls the flow of carrier gases transporting the gaseous precursors; a reaction chamber, often a quartz tube, where the growth process takes place; a high-temperature furnace surrounding the reactor providing thermal energy for the chemical reactions; and an exhaust system. Some CVD systems are equipped with a plasma generator to increase the reactivity of certain gas precursors, separate heating elements for precursors with low evaporation temperature, such as sulphur, or bubblers for liquid precursors.

Edge epitaxy, crucial for in situ production of lateral heterostructures, has been achieved by different CVD modifications.[44-53] Similar structure and chemistry among the TMDs generally promote alloy formation.[60-62] Hence, a one-step direct growth with all precursors simultaneously

present in the reactor requires separating in time the deposition (or nucleation) of the different components of a lateral heterostructure. Early one-step CVD approaches made use of distinct evaporation thresholds and kinetics of molybdenum and tungsten precursors;[49] a heterojunction is formed due to early evaporation and then depletion of the molybdenum precursor followed by slower evaporation of the tungsten precursor. A major limitation of this approach is that only one junction can be formed, which is furthermore compositionally graded (alloyed). Growth of the different components in separate CVD reactors achieves atomically sharp interfaces and provides additional flexibility in combining TMDs that contain different metal and chalcogen species such as WSe_2-MoS_2.[51]

CVD synthesis of TMD multi-junction lateral heterostructures and superlattices Multiple lateral heterojunctions or superlattices have a high level of complexity as they require the controlled cyclic growth of the individual domains. At least three different CVD strategies have successfully produced such multi-junction heterostructures.[46,52,53]

In standard CVD, where the precursors originate from the evaporation of powders at high temperature, a major drawback is the uncontrolled nucleation during temperature ramps before and after the growth. This issue can be addressed by a gas supply system where, depending on valve configurations, either side of the reactor can function as gas inlet or outlet (Figure 4a).[53] The gas flow is reversed from substrate to source during temperature ramps to prevent undesired nucleation or thermal degradation. Once the growth temperature is reached, the flow direction is switched to transport the vapor phase precursors from the source to the substrate and initiate controlled growth. Based on this process, the lateral growth of each component of a heterostructure is carried out in separate CVD systems, choosing optimal conditions of temperature and gas flow for each material.[53] While requiring sequential CVD steps to synthesize multi-junction heterostructures, this method has the advantage of suppressing cross-contamination and uncontrolled homogeneous nucleation.

In water-assisted one-pot CVD,[46,47] source powders of two TMD compounds with different metal atoms (for example MoS_2 and WS_2) are placed in the same crucible (Figure 4b). During temperature ramping, the reactor with substrates and powders (kept under nitrogen flow) remains outside the furnace to prevent undesired evaporation and nucleation. Once the growth temperature is reached, the quartz reactor is slid into the furnace so that the powder sources are in the highest temperature zone and the substrates in their growth temperature zone. Water vapor, introduced in the reactor by passing nitrogen through a bubbler, reacts with the TMD powders, promoting the formation of volatile oxides and hydroxides that are transported to the substrates together with the chalcogen precursors. To separate the nucleation of different components of a heterostructure, differences in oxidation levels and oxidation/reduction kinetics of the molybdenum and tungsten compounds are exploited. In general, the oxidation/reduction kinetics of molybdenum is faster than for tungsten. During the reaction with water, molybdenum forms oxides that can subsequently deposit on the substrate. Tungsten preferentially forms hydroxides that are highly volatile and will not adsorb on the substrate. Therefore, under N_2/H_2O gas only molybdenum oxides adsorb on the substrate and produce molybdenum-rich TMD domains. Upon switching the carrier gas to argon/H_2, the supply of molybdenum oxides is rapidly depleted while tungsten oxide precursors continue to be delivered due to their slower reduction rates. Hence, argon/H_2 gas promotes the growth of tungsten-rich TMD domains. The synthesis of multi-junction heterostructures involves repeatedly switching the carrier gas between N_2/H_2O and

argon/H_2. This method proved to be effective in producing periodic TMD heterostructures whose components contain different metals but similar chalcogen composition, including those containing ternary alloys with mixed chalcogens.[63]

Low-pressure CVD with metal-organic precursors can provide excellent control over the domain size (down to 20 nm) and reproducibility to form lateral superlattices (Figure 4c).[52] The precursor gases are introduced into the reactor through individual mass flow controllers. Tungsten hexacarbonyl and molybdenum hexacarbonyl, used as precursors for tungsten and molybdenum, respectively, are kept in bubblers while passing argon as the carrier gas. Diethyl sulfide and dimethyl selenide are the sulphur and selenium precursors. Additional H_2 and argon carrier gases are introduced during growth. Heterostructures where only the chalcogen changes are realized by alternating the flow of the sulphur/selenium precursors, with breaks for purging purposes.

Patterned regrowth methods[17] have proven to be effective for controlling the geometry and periodicity of arbitrary-shaped and multi-junction heterostructures. A popular approach uses SiO_2 mask patterns, defined by electron beam lithography on CVD-grown 2D $MoSe_2$.[54,55] The patterned sample is then exposed to sulphur precursors at high temperatures to promote chalcogen exchange in the exposed regions. Reactor pressure and sulphur source vary, ranging from high vacuum and laser-evaporated sulphur[54] to the few Torr range and thermally evaporated sulphur powder;[55] the process temperature needs to be optimized to achieve complete chalcogen exchange and avoid ternary alloys (low T) or crystal damage (high T). An alternative process uses resist-free focused ion beam patterning to etch selected regions of a 2D TMD (such as WS_2), thus creating exposed edges that serve as seeds for lateral epitaxy of a second TMD (such as WSe_2).[56]

Direct CVD synthesis of vertical heterostructures

In contrast to mechanical stacking and growth of lateral heterostructures, the direct synthesis of vertical heterostructures has remained less explored due to intrinsic limiting factors such as different temperature stability and/or chemistry of the 2D materials to be combined. Some of the single-step and multi-step CVD processes for lateral integration have also been utilized to produce vertical stacks. In single-step CVD, for instance, vertical growth is promoted by higher temperatures compared to the conditions producing lateral heterostructures.[48] Higher growth temperatures provide the kinetic energy needed for the adatoms of the second component to overcome the edge energy barrier[47] and climb to the surface of the first layer. When all precursors are simultaneously present in the CVD reactor, some alloying or cross-contamination is inevitable. Multistep CVD approaches where the different materials are grown separately are therefore preferred for vertical stacks since they minimize alloying and provide better domain control.[64,65] A disadvantage of the direct synthesis of vertical heterostructures is that even in a multistep approach, the materials that require higher synthesis temperature must be grown first to minimize thermal decomposition or alloying during the following synthesis steps. This considerably restricts the possible materials combinations in synthetic vertical stacks.

Emerging materials, unconventional geometries, and natural heterostructures

Graphene, h-BN, and TMDs lend themselves well to creating vertical van der Waals stacks either by mechanical stacking or bottom-up synthesis, and for growing lateral heterostructures.[18,43,45,49,50] Synthesis of vertical stacks and lateral heterostructures is facilitated by the ease of growing and isolating monolayers, the straightforward polymorphism of these

materials,[66] and the fact that they exist with fixed stoichiometry (for example, MX_2 for TMDs). Layered crystals that deviate from these characteristics present opportunities for creating unconventional types of heterostructures. A prominent example are group IV (tin, germanium) chalcogenide semiconductors, which can crystallize in distinct layered phases with different chalcogen content. Tin sulfides, for example, exist as SnS_2, Sn_2S_3, and SnS, all of which have different functional properties. SnS_2 is a trigonal 2D/layered dichalcogenide (space group $P\bar{3}m1$) with high carrier mobility in field effect transistors[67] and promise as a photocatalyst.[68] Monochalcogenides such as SnS (or generally MX, where M: tin, germanium; X: sulphur, selenium) are orthorhombic crystals (space group *Pnma*) with anisotropic transport,[69] optoelectronics,[70] and valleytronics[71] along with other exceptional properties such as in-plane ferroelectricity.[72,73]

The tunability of stoichiometry and structure via the chalcogen chemical potential can be exploited to obtain van der Waals heterostructures. Reduction of dichalcogenide crystals by inducing chalcogen vacancies produces heterostructures of MX embedded in a MX_2 matrix.[74] Growth of monochalcogenides with excess chalcogens leads to coexisting MX and MX_2 phases. The incompatibility of their crystal structures drives phase separation, producing layered wrap-around core-shell heterostructures, for example of a crystalline SnS core surrounded in a seamless SnS_2 shell.[75] Abundant type II interfaces in these core-shell structures reduce the optical absorption edge to 0.65 eV, below the bandgap energies of both SnS (1.2 eV) and SnS_2 (2.2 eV) by excitation of interfacial electron-hole pairs, providing an effective approach for infrared sensitization in light harvesting applications.

Isostructural group IV monochalcogenides and their alloys provide other avenues for synthesizing heterostructures. Due to their open structure and enhanced surface reactivity,[76,77] materials such as SnS tend to grow as thicker (> 50 nm, or about 100 layers or more) multilayer crystals. With vertical {110} side facets,[78] such crystals can act as seeds for the lateral epitaxy of a second monochalcogenide (such as GeS), creating lateral heterostructures analogous to those realized with 2D TMDs but with sharp, atomically connected lateral interfaces that extend across many individual van der Waals layers.[79,80] Another frontier, shaping 2D/layered crystals into the third dimension, can be pursued by exploiting the lattice mismatch between different monochalcogenides. $Ge_{1-x}Sn_xS$ alloy nanoribbons whose edges are enriched in SnS experience compressive edge stress, which in turn induces controlled **axial twisting**.[81] Their unique geometry with continuous transition between planar and vertical orientation, along with their ability to carry propagating polariton modes make such 3D-shaped nanoribbons promising for transduction of energy and information.

In contrast to artificial, engineered heterostructures, some materials occur naturally as bulk crystals comprising ordered stacks of van der Waals layers. Found in the earth's crust as minerals, such natural van der Waals heterostructures show excellent stability in air and provide a convenient starting material for exfoliating few-layer heterostacks. Franckeite, for example, is a layered sulfosalt mineral consisting of alternating tin disulfide (SnS_2) and lead sulfide (PbS) based layers. Its exfoliation produces p-type semiconducting few-layer heterostructures with narrow bandgap[82,83] and broad-band photoresponse.[84] With their diversity in crystal structure and chemistry, franckeite and other sulfosalts,[85,86] phyllosilicates,[87] and other minerals provide a rich family of bulk crystals for exfoliating ultrathin, air-stable, and adsorbate-free van der Waals stacks.

Controlling interlayer twist in synthetic homo- and heterostructures

Since conventional rules on materials compatibility and lattice matching governing ordinary epitaxial growth no longer apply in van der Waals heterostructures, stacking of layered (or non-layered) crystals can overcome key limitations that have hindered integration of 3D crystals in heterostructures. In addition, van der Waals stacking opens up new degrees of freedom that are inaccessible in 3D crystals. In particular, instead of assuming a fixed orientation, homo- or heterolayers can be stacked at arbitrary azimuthal angles between their lattices. Such interlayer twist not only affects the interaction and equilibrium separation between the layers,[88] but it also modulates their electronic coupling.[89] In bilayer graphene, small twists near a **magic angle** of ~1.1° give rise to flat electronic bands close to the Fermi energy, causing strong electron correlations and emerging many-body phenomena.[90,91]

Twisted van der Waals stacks have been fabricated almost exclusively by mechanical stacking,[92] and it has proven challenging to develop scalable synthesis strategies that provide control over the twist angle. The difficulty of achieving twisted stacking in van der Waals epitaxy is illustrated by calculations for bilayer graphene, which show a deep energy minimum for equilibrium A-B (or Bernal) stacking, in which the B-atom of the two-atom unit cell of the second graphene layer is stacked atop the A-atom of the first layer; experiments confirm a thermally activated rotation of twisted layers back to the equilibrium alignment.[93] A possible way of inducing interlayer twist involves growth away from equilibrium. Forcing a hetero-site nucleation during graphene CVD on copper enabled the nucleation of the second layer at a different site from that of the first layer, so that a majority of the second-layer nuclei adopted a distinct orientation.[94] This stochastic process produces predominantly twisted bilayer graphene but it does not provide control over the twist angle.

Several alternative approaches have been developed to address this critical shortcoming. For example, spiral growth on curved non-Euclidean surfaces can result in helical multilayer superstructures with twisted van der Waals interfaces. Growing WS_2 or WSe_2 on substrates with protruding nanoparticles shows twisted spirals whose interlayer twist is in principle tunable via the shape of the substrate (Figure 5a).[95] Another approach toward growth of twisted stacks involves a two-step van der Waals epitaxy, in which the final orientation of a growing crystal is not defined by lattice-alignment with the substrate, as in ordinary epitaxy, but is inherited from a sacrificial intermediate (Figure 5b). Growth of a sacrificial intermediate crystal with fixed azimuthal orientation to the substrate lattice has been realized with SnS on different non-isotypic substrates including SnS_2, MoS_2, and WS_2.[96] In the second step, the SnS intermediate is transformed to SnS_2 by solid-state sulfurization. Since its orientation is defined by the SnS intermediate, the final trigonal SnS_2 crystal is consistently 30° twisted relative to the substrate lattice, and repetition of the process can produce twist superlattices with 30° rotation at each interface.

Tunable and stable small-angle interlayer twists can be realized by abandoning a planar geometry. **Eshelby twist**[97] in van der Waals nanowires hosting axial screw dislocations produces chiral growth spirals with interlayer twist $d\theta/dz = \boldsymbol{b}/[\pi R^2]$ that is tunable via the radius R of the wire ($\boldsymbol{b}$ is the Burgers vector of the dislocation).[98] In vapor-liquid-solid nanowire growth, R follows the size of the growth catalyst, meaning it can be adjusted precisely via the choice of the metal nanoparticle catalysts. For the twisted GeS van der Waals nanowires realized to date, R ranges from over 100 nm down to ~7.5 nm, which for a single unit cell Burgers vector translates

into interlayer twists from below 0.002° to 0.32°.[99] This approach for realizing precision tunable interlayer twists has several unique aspects: Small interlayer twists are effectively stabilized by the screw dislocation; the resulting twist moiré is projected onto a helicoid rather than a planar surface, its footprint is usually much smaller than the moiré unit cell, and a progression of different moiré registries (and associated electronic properties) is found along the nanowire axis;[98] and the unusual geometry enables features such as continuously varying interlayer twists and twist homojunctions that are impossible to realize in a planar topology.[100]

Results

Both vertical and lateral heterostructures present challenges in characterization, since their characteristic length scales span from atomic scale interface regions to several tens of micrometer overall dimensions of a typical sample. Generally, multiple techniques are applied to obtain a complete picture of structure, chemical composition and properties. They range from simple approaches such as optical microscopy to advanced methods including electron microscopy, scanning probe methods and optical approaches such as Raman and photoluminescence spectroscopy.

Structure analysis

Overall sample morphology

A simple technique for quick routine inspection of the distribution, density, shapes and domain sizes is optical microscopy. 2D materials are well visualized when deposited on SiO_2/silicon substrates with 280-300 nm oxide thickness. The contrast is mainly explained by multilayer optical interference[101-103] and depends on both the layer thickness as well as the optical constants of the materials. The 2D lateral heterostructure in Figure 6a, prepared using water-assisted CVD,[46] show clear optical contrast between MoX_2 (darker) and WX_2 (lighter) domains. Scanning electron microscopy (SEM) offers nanometer spatial resolution and allows visualizing details (for example, narrow TMDs domains, see Figure 6a)[52] based on a different attenuation of secondary electrons emitted from the underlying substrate. Scanning probe methods such as atomic force microscopy (AFM) and its different imaging modes[104] are useful tools for rapid screening of sample morphology, precise thickness measurements, and for measuring properties such as surface potential, mechanical stiffness. The AFM image in Figure 6a of a 2D lateral superlattice shows the average height of the heterostructure, along with out-of-plane ripples in the WSe_2 domain due to strain resulting from the lateral bonding to the mismatched WS_2 domains.[52] Ex-situ imaging techniques are complemented by in-situ imaging, such as using environmental SEM,[105] scanning transmission electron microscopy (STEM),[106] and low-energy electron microscopy (LEEM).[107] Among these approaches, LEEM is particularly powerful since it provides real-time imaging of the growth processes underlying heterostructure formation,[96] combined with local crystallography via electron diffraction, surface potential mapping,[108] and even local band structure measurements.[109,110]

Atomic-scale structural and chemical analysis

Transmission electron microscopy (TEM) and STEM are unrivaled in their ability to image crystal structure, defects, interfaces, stacking registry, twist moiré patterns and other important characteristics of van der Waals heterostructures with atomic resolution. For samples supported on conducting substrates, scanning tunneling microscopy gives access to atomic-scale structure,

and tunneling spectroscopy provides information on the electronic structure (for example, local density of states, bandgaps, band alignments) down to the atomic scale and is therefore widely used to investigate 2D heterostructures, defects, interfaces, or twist moirés.

High-angle annular dark-field (HAADF) STEM has become a routine tool for visualizing the crystal structure and defects in 2D materials, as well as the quality of lateral hetero-junctions at the atomic level. Using probe aberration correction, sub-Å spatial resolution is obtained, so that lattice structure and individual point defects are readily imaged. Using this Z-contrast imaging, combined with electron energy loss spectroscopy (EELS), intermixing near interfaces can be quantified with single-atom resolution as illustrated in Figure 6b for a monolayer lateral heterostructure.[46] High-resolution TEM provides similar information, but requires image simulations to interpret the contrast as it lacks the intuitive interpretation of image contrast as in HAADF-STEM. Figure 6b illustrates the capabilities of atomic-scale TEM imaging with the example of a complex interface between a few-layer SnS core that is seamlessly wrapped in a layered SnS_2 shell.[75] Real-space imaging is further complemented by local crystallography using electron diffraction, which in the form of nanobeam diffraction can give structural information for nanometer-scale regions of interest.[98,99]

Finally, the focused probe in STEM can enable a number of additional analytical modes, notably EELS and energy-dispersive spectroscopy (EDS), which provide spatially resolved elemental and chemical analysis of heterostructures. In Figure 6b, EDS chemical mapping is used to discriminate between the different components of a SnS-GeS multilayer lateral heterostructure.

Vibrational and optoelectronic properties

Spatially resolved measurements

Raman and photoluminescence spectroscopies measured in a confocal optical microscope have become key techniques to study 2D materials in general. Both Raman and photoluminescence can be measured in the same experimental setup, where the samples are excited by a focused laser and the scattered or luminescence light is analyzed in an optical spectrometer. The Raman signal contains information about vibrational modes (phonons) that are unique to each material, and it is affected by chemical composition, number of layers, local strain fields and electronic doping. Photoluminescence spectroscopy offers information about electronic transitions; due to reduced screening in 2D and the resulting large exciton binding energies, photoluminescence spectra of 2D materials and heterostructures are often dominated by the recombination of free-excitons, bound-excitons, biexcitons, or trions. Photoluminescence is also sensitive to strain, temperature, the dielectric environment, doping and defects. As diffraction-limited optical techniques, Raman and photoluminescence can be measured with spatial resolution of few hundred nm and local signals can be assembled into sub-μm resolved maps as shown in Figure 6c. To further enhance the spatial resolution, near-field optical techniques or sub-diffraction excitation can be used. Scanning near-field optical microscopy, for example, using a sharp metallic probe in close proximity of the sample to obtain strong field-enhancements of scattered radiation, has become a versatile method for probing light-matter interactions across broad spectral ranges from the visible to the mid-infrared and THz in 2D materials,[111] heterostructures,[112] and twisted stacks[113] with tens of nm spatial resolution. Similarly, tip-enhanced Raman and photoluminescence spectroscopies,[114] allow investigating phonons and luminescence below the diffraction limit (see Figure 6c). An alternative to tip-based near-field optical methods is provided by measuring luminescence excited by a focused electron beam.

While the most widespread method, cathodoluminescence in SEM (SEM-CL), provides ~10 nm scale excitation, using the focused electron beam in STEM allows excitation in 1 nm sized regions of interest. Such STEM-CL can readily accommodate challenging geometries, such as the 3D-shaped heterostructure shown in Figure 6c.[80] It is important to note that only the excitation in STEM-CL is local; light collection occurs in the far field. This implies that the excitations (electron-hole pairs or excitons) can undergo diffusion and drift before recombining, providing a powerful tool for the investigation of exciton diffusion lengths[115] and interfaces in van der Waals heterostructures.[79,80] Coherent excitation by the electric field of the traversing electron beam can also stimulate photonic waveguide modes and propagating polaritons.[80,116-118] Finally, cathodoluminescence is nicely complemented by atomic-scale absorption measurements by monochromated EELS to realize a full analysis of optical absorption and light emission at the nanoscale.[100]

Applications

Photonics and plasmonics

The development of deterministic placement methods for assembling van der Waals stacks opened the door for fabricating heterostructures of arbitrary 2D (or even 3D) materials with atomically sharp and clean interfaces, regardless of crystal structure or lattice mismatch. This advance has enabled the fabrication of exotic pn-junctions that leave virtually no space for a depletion region yet display a strong photovoltaic effect,[119-121] or efficient light emitting diodes based on complex quantum well stacks with engineered band structure.[122] Such optoelectronic devices carry large potential for applications requiring flexible and quasi-transparent devices. Apart from the fabrication of devices based on heterostacks, deterministic placement methods also allow for the fabrication of stacks where the crystal alignment between the constituent layers is accurately controlled. This opens up a new field of research, twistronics, where interlayer twist moiré patterns give rise to exotic electronic and optical properties. An example of the latter is the observation of unconventional features in the photoluminescence spectra of heterostructures of different semiconducting TMDs. These features have been attributed to the potential landscape arising from the **moiré potential** generated by the twisted stacking of dissimilar (lattice-mismatched) TMD layers.[123-128]

Van der Waals heterostructures have been widely studied for plasmonics. The most explored system are heterostructures formed by graphene and h-BN. Graphene is known to be an ideal medium, supporting surface plasmons with high confinement, gate tunability, and a broad spectral range from infrared to terahertz. Nevertheless, surface plasmons in graphene supported on ordinary substrates at ambient conditions have shown high damping due to a relatively low carrier mobility.[111,129] Encapsulating graphene between h-BN flakes (Figure 7a) can significantly improve the mobility of graphene, and thus reduce the loss of graphene plasmons.[130,131] As shown in Figure 7b, the propagation length of graphene plasmons can then exceed ten μm at low temperatures.[131] Such low-loss infrared plasmons enabled by the heterostructure can lead to important technological applications, such as terahertz detection.[132] Graphene/h-BN heterostructures are commonly created by mechanical transfer, so the lattices of the two materials are incommensurable. In the case of commensurable structures grown by CVD, moiré superlattices form, which modulate the electron wavefunction and generate satellite **Dirac cones**.[133] This unique electronic structure leads to intriguing plasmonic responses, where free

electrons from the normal Dirac band are in concert with interband transitions close to the sub-Dirac cones.

Besides graphene/h-BN, there are many other heterostructures with unique plasmonic functionalities. For example, pentacene/graphene heterostructures (Figure 7c, d) have shown a reduced plasmon wavelength and hence a higher plasmonic confinement compared to bare graphene.[134] This is attributed to a charge transfer between graphene and molecular layers of pentacene causing reduced graphene doping. Effects of interlayer charge transfer are also detected in graphene/α-$RuCl_3$ heterostructures, where the graphene doping is enhanced.[135] Due to the high doping, plasmons are observed at significantly higher frequencies than for graphene on SiO_2 or SiC.[111,129] In both pentacene/graphene and graphene/α-$RuCl_3$ heterostructures, the charge transfer originates from a work function difference between the interfacing materials. Compared to electrostatic or chemical doping, charge transfer is convenient, non-destructive, and it can create stable doping regions with sharp boundaries. Patterning the charge donor or acceptor can in principle create periodic potentials, needed to realize graphene plasmonic crystals – the plasmonic version of photonic crystals[134].

Another way of tuning plasmonic response involves graphene/dielectric/metal heterostructures (Figure 7e), where graphene and a metal layer are separated by a dielectric spacer. Typically, gold is used for the metal layer, and h-BN or Al_2O_3 as the dielectric spacer. Coupling between metal and graphene causes a linear dispersion of surface plasmons in the heterostructure, so they are termed acoustic plasmons (Figure 7f).[136] These plasmons show a reduced wavelength and hence higher lateral confinement. Optimal plasmon confinement can be achieved when using atomically thin h-BN as the spacer.[112] In this case, the plasmon field existing mainly in the gap between graphene and gold is strongly confined vertically and hence significantly enhanced. With such extreme confinement and field enhancement, acoustic plasmons are promising for ultrasensitive infrared detection and sensing.[137]

Stacking 2D and 3D crystals

Although research on van der Waals heterostructures has focused on 2D/layered crystals, the concept applies much more broadly since the van der Waals force represents a general intermolecular interaction between any two objects placed in close proximity. By avoiding chemical bonding, van der Waals stacking offers unprecedented freedom for integrating dissimilar materials into engineered heterostructures unconstrained by lattice matching requirements.[138,139] Preformed components can be picked up, transferred, and laminated without interfacial contamination, thus largely preserving the intrinsic electronic properties of the constituents.[140-142]

Early efforts of van der Waals integration focused on transferring high-κ dielectrics onto delicate channel materials, such as graphene and 2D semiconductors, to form interfaces with little chemical disorder and trap states, essential for efficient electrostatic gating.[143-145] For example, the transfer of synthetic Al_2O_3 nanoribbons on graphene created top-gated graphene field-effect transistors with atomically clean dielectric interfaces and high carrier mobility.[143] Integration of metal-dielectric core-shell nanowires or a lithographically defined gate stack produced graphene[140,144] and MoS_2[146] transistors with ultrahigh intrinsic cutoff frequencies. Van der Waals integration of a silver iodide superionic gate allows programmable ionic doping of 2D materials and enables temporary and delible electronics desirable for electronic security.[147]

Beyond passive dielectric interfaces, van der Waals integration can also create active, current-carrying metal/semiconductor junctions. For example, transfer of lithographically fabricated metal thin film electrodes onto 2D semiconductors produces nearly ideal junctions with atomically clean, pinning-free interfaces that perform near the Schottky-Mott limit,[141] which has been difficult to achieve in traditional metal/semiconductor junctions.[148] Such pinning-free van der Waals contacts can be exploited to realize nearly ideal photodiodes with negligible interfacial recombination and unity internal quantum efficiency.[149]

Besides 2D materials, van der Waals stacking can be applied to different (3D) bulk crystals, to obtain damage-free contacts to delicate materials such as lead halide perovskites that are easily degraded during lithography or metal deposition.[150] Van der Waals integration of gold contacts on $CsPbBr_3$ minimizes interfacial disorder, enabling record carrier mobilities and low bimolecular recombination rates.[151] The integration of platinum on β-Ga_2O_3, producing metal-semiconductor field-effect transistor rectifiers with designed barrier height, highlights the generality of van der Waals stacking for creating heterostructures with designed electronic interfaces.[152]

Van der Waals forces can also be used to create superlattices between radically different materials, such as covalently bonded 2D crystals and self-assembled molecular layers. The weak coupling between neighboring layers inherently relaxes interfacial strain, retaining nearly perfect crystallinity regardless of structure differences. This is in stark contrast to conventional (epitaxial) films and superlattices, where even a small lattice mismatch can induce morphological changes[153] or misfit dislocations.[9] The ability to integrate such different materials promises new generations of engineered materials with tailored electronic, magnetic or topological properties. For example, superlattices of alternating black phosphorus and cetyltrimethylammonium bromide (CTAB) were created by electrochemical intercalation.[142] The intercalated CTAB layers spatially separate and electronically decouple the atomic layers in black phosphorus, thus producing a bulk material with monolayer physical characteristics. Expanding such artificial van der Waals superlattices to other layered hosts and designer intercalants can create a rich library of engineered materials with tunable structure and function.[154]

Twisted stacks

Van der Waals stacks overcome the compatibility limitations of conventional epitaxy, thereby providing exceptional opportunities for materials integration and opening up new degrees of freedom such as interlayer twist. Graphene/h-BN stacks with twist angles close to 0° were among the earliest such heterostructures, which due to the lattice mismatch between the components showed a modulation of the electronic structure of graphene manifest via superlattice resistance peaks[155-158] and Hofstadter fractal structure.[156,159] Due to the large difference in band structure between graphene and h-BN, however, there is no electronic coupling between the two materials.

Arguably the most intensely studied ultrathin van der Waals system is twisted bilayer graphene (TBG). A relative azimuthal lattice rotation of the two layers in TBG produces a periodic moiré superlattice, for which theoretical calculations predict flat electronic bands near the Fermi energy for a twist angle of 1.1°.[16] However, fabricating and stabilizing such magic angle twisted bilayers poses significant challenges. The challenge of mechanically stacking the graphene layers with a precise relative twist angle can be overcome by using the tear and stack (or the related cut and stack) method, in which part of a single 2D flake is torn off (or cut by an AFM tip or laser),

picked up, and transferred with a defined rotation onto the remaining half of the flake.[92,160] Another difficulty is related to the fact that A-B stacked graphene is the lowest energy configuration, while layers stacked with a small twist tend to spontaneously switch back into 0° alignment if sufficient thermal energy is supplied.[161-163] If this issue is overcome, for example by keeping the thermal budget at a minimum following the twisted stacking of the layers, a broad range of exciting physics opens up in the stacked carbon layers. Magic-angle TBG indeed shows flat electronic bands with Fermi velocity only $1/25^{th}$ of that in monolayer graphene. The weakly dispersive bands favor strong electron interactions, which lead to emerging many-body phenomena including superconductivity and Mott insulating behavior.[90,91] A beautiful aspect of the strongly correlated electron system in magic angle TBG is the facile adjustment of the carrier concentration by electrostatic gating, in contrast to the chemical doping required in conventional superconductors. Gated transport shows an insulating gap at half-filling of the flat band, which turns into a metallic state as temperature is lowered to 4 K. Superconductivitiy is found near the correlated insulating state at half filling, with a transition temperature of 1.7 K.[91] A superconducting state can also be induced by applying high pressure in TBG with 1.27° (non-magic) twist angle, due to enhanced interlayer coupling at high pressure.[164] As the quality of the twisted samples improves, magic-angle TBG with enhanced uniformity allows additional features such as resistance peaks at 1/4 and 3/4 filling to be observed. Finally, flat bands with electric field tunable carrier density are also found in twisted double-bilayer graphene (TDBG),[165-167] which shows signs of superconductivity-like phenomena.[165] However, the resistance of TDBG does not reach zero below the transition temperature, leading to the hypothesis that it has a distinct ground state different from the superconducting state.[168]

Although less explored than TBG, twisted TMDs are beginning to attract significant attention. In twisted WSe_2 bilayers for example, an associated insulating state is found for a larger twist angle range than in TBG,[169] and twisted WSe_2/WS_2 heterostructures show Mott insulating and Wigner crystal states.[170,171] Twisted bilayers of semiconducting TMDs also display a variety of optoelectronic phenomena linked to the modulation of the electronic structure by a periodic twist moiré pattern, including for example moiré excitons in WSe_2/WS_2,[172] $MoSe_2/WS_2$[128] and $MoSe_2/WSe_2$[126,127] twisted hetero-bilayers.

Theoretical calculations predict emerging moiré physics for other materials systems, including twisted bilayer h-BN[173] and bilayer GeSe,[174] showing that they can also realize flat bands at small twist angles. More broadly, it has been suggested that flat band moirés can be used as quantum simulation platforms for the study of strongly correlated systems of different symmetry, such as 2D triangular lattices, honeycomb lattices, and quasi 1D lattices.[175] While there are still many open questions about the emerging phenomena, 2D materials based twisted stacks have clearly opened up a new branch of condensed matter physics, which promises new insight into strongly correlated systems as well as other electronic and photonic phenomena arising as a result of long-range moiré superlattices.

Reproducibility and data deposition

Reproducibility can be an issue in experiments relying on van der Waals heterostructures fabricated by manual mechanical assembly. The skills of the operator, experimental setup and details of the techniques employed in the fabrication are all variables that need to be considered. A more thorough description of the experimental setup and tools employed is desirable to enhance the reproducibility of results. Currently, most articles only include references to past

work, while the actual setup and techniques have been revised (sometimes only slightly) further since the publications of those references. Thus, the descriptions provided are usually not sufficiently accurate or detailed to allow for a complete understanding of the methods or full reproducibility of the results. Different issues arise with novel van der Waals heterostructures, such as twisted stacks. Here, homogeneous twist angles are usually obtained only at limited scale, typically a few μm or smaller in size. Differences in observed spectra for moiré excitons, for example, can be explained by a strong dependence on the possibly inhomogeneous interlayer rotation angle.[126-128,172] The heterogeneity in interlayer twist tends to be difficult to characterize and so is not fully reported in publications. This issue calls for the development of characterization techniques that allow measuring/mapping interlayer twist across all relevant length scales. As exfoliation and stacking methods mature, a larger emphasis will also need to be placed on the quality of the source materials since it will increasingly limit the homogeneity and size of the achievable structures. Addressing this issue calls for optimization of crystal growth for layered bulk materials. Long term, it is likely that bulk crystals will be replaced by synthetic monolayers, which after isolation from their growth substrates can provide exceptionally large (up to wafer scale), homogeneously thin starting materials for the assembly of van der Waals heterostructures.

Similar issues hamper reproducibility in the case of van der Waals systems synthesized by bottom-up approaches. The growth systems generally follow similar designs, comprising a quartz tube reactor heated inside a tube furnace with one or several independently controlled temperature zones, and with a controlled carrier gas flow. All too frequently, the reported methods used for growing 2D materials and heterostructures include incomplete information. For example, for single-zone furnaces only the precursor temperature is specified, while the substrate temperature is represented via the distance of the samples from the source crucible. Given the differences in size, insulation, nominal length of the heated zone and temperature profile between different furnaces, this information makes it virtually impossible to reproduce the results of the synthesis without tedious experimentation to replicate the growth conditions. To achieve broad reproducibility, a standard should be enforced where both the relative position of source and sample and the entire temperature profile between them are reported in the methods. As a minimum, measured temperatures at the position of the source and substrate(s) should be given along with the distance between them. Even with this information provided, additional experimentation will typically be required to replicate a growth reported for a different laboratory and setup. Additional factors that complicate reproducibility in synthesis include small differences in furnace temperature profiles and thermal inertia, laboratory temperature and humidity, specific procedures used during heating and cooling ramps (such as ramp rates, types and flow rates of gases during the ramping stages), quartz reactor diameter and cleaning procedures, and methods of substrate preparation, cleaning and handling.

As in many other fields, progress in both technique development for fabricating van der Waals heterostructures and in understanding their properties may be accelerated by enhanced transparency and data sharing. One complication is the lack of minimum reporting standards for structural and chemical analysis, as well as for measurements of functional properties. Sharing is also complicated by the use of proprietary software for data acquisition, notably in areas with large data volumes such as microscopy. Making such data (and the associated metadata) available to the scientific community and the public may require the deployment of reader software that allows unlicensed users to access raw data stored in proprietary formats.

Limitations and optimizations

Automated robotic assembly of stacks

Compared to bottom-up techniques, the manual stacking of 2D (and 3D) materials has the major advantage of offering complete flexibility in the geometry of the assembled stacks. Using deterministic placement methods, van der Waals stacks can be fabricated without constrains arising due to crystal structure or chemical composition of the constituent layers. This provides complete freedom in the fabrication of artificial matter with virtually infinite combination possibilities. These advantages strongly motivate efforts to find new ways to overcome the main limitation of the top-down deterministic placement approach: The reliance on tedious manual procedures to identify the constituent 2D flakes, align them as desired and assemble them into a van der Waals heterostructure. With such a manual process, the quality of the produced stacks can vary from sample to sample, and can depend on the researcher performing the assembly.

One straightforward way to eliminate this dependence on visual recognition and manual assembly is to replace the human operator by a combination of computer algorithms and motorized stages to perform the same tasks. In 2018 it was demonstrated how such a system can be implemented.[176] A fully automated setup identified 2D materials through image processing and artificial intelligence, then transferred them onto the desired position with high accuracy using motorized stages, thus performing the entire assembly process without the intervention of a human operator. This approach, although unlikely to be brought up to industrial scale, clearly constitutes an important step toward improving both the reliability and the achievable complexity of samples prepared by top-down deterministic transfer methods.[177] Enhancements in reliability, reproducibility, homogeneity and complexity made possible by robotic assembly, ultimately extended to controlled environments or ultrahigh vacuum, may become crucial when studying exotic physical phenomena occurring on stacks of 2D materials twisted by a small angle where the sample-to-sample variability can hamper a thorough understanding of the system.

Synthetic heterostructures

CVD methods each have their own advantages and disadvantages. The reverse flow approach,[53] for instance, is efficient in producing sharp heterojunctions without intermixing or cross-contamination. Additionally, this approach is superior in its versatility in combining all the TMDs available in the molybdenum and tungsten family. A disadvantage is that every material must be grown in a separate CVD reactor. Since the preparation of each synthesis experiment can take several hours, including heating and cooling ramps, growing a complex multi-junction heterostructure or superlattice can take days. The reproducibility of the domain size in lateral heterostructures is yet to be assessed. On the other hand, water-assisted one-pot CVD[46] can produce complex heterostructures and superlattices in a single synthesis run by switching the carrier gas. In water-assisted one-pot CVD, [46] reproducible domain size was demonstrated, producing heterostructures based on sulfides, selenides, and ternary alloys. However, water-assisted CVD can only be used to grow heterostructures with different metal species from one domain to another, and some of the junctions are not as sharp as in the reverse flow method. Additionally, special care must be taken with the water temperature in the bubbler, and a thermal bath is recommended if alloying of the metal element is to be avoided. Modulated metal-organic CVD,[52] proved to be reproducible and controllable even for very narrow domains. One disadvantage of this method can be the use of hazardous precursors that require extra safety precautions and infrastructure.

Most of the limitations affecting the scalability of CVD approaches are related to the use of horizontal tube furnaces with gradients of temperature as well as of the spatial distribution of products across the reactors.[178] The industrial production of 2D heterostructures over large areas with homogeneous sample quality and morphology will require redesigning the furnace geometry and strategy for delivering precursors. For instance, furnace reactors with planar geometry, laminar flow and large-area temperature plateaus will guarantee homogeneous growth conditions over large areas. If metal-organic precursors are to be avoided, upstream solid powder sources should be homogeneously distributed across the reactor cross-section to avoid spatial concentration gradients in the carrier gas. Alternative strategies could also consider vertical versus horizontal CVD geometries.[179]

Outlook

As a vital part of the top-down preparation of 2D crystals and heterostructures, exfoliation from layered bulk crystals will continue to see further development and enhancement benefiting both basic research and applications. Directions for future development include approaches to achieve larger crystals of higher quality, taking advantage of improved control over interfacial interactions as demonstrated by gold-assisted exfoliation and requiring crystal growth processes that yield optimal quality of the source bulk crystals at large (wafer) scale.

The deterministic assembly of van der Waals heterostructures by mechanical stacking faces two main open challenges. The first and perhaps most pressing challenge is to decrease the amount of residues trapped between the stacked layers that tend to form bubbles and ripples, limiting the effective clean surface area in which one can fabricate a final device.[180,181] In fact, there are already experimental demonstrations of the possibility of fabricating heterostructures under high vacuum, but the implementation of these systems is still not widespread and the transfer method requires the 2D materials to be exposed to air during some steps of the heterostructure assembly.[182,183] The development of cleaner transfer methods or the implementation of these techniques in a controlled ultrahigh vacuum environment will be one of the research directions of the near future. The second open challenge, which does not have an obvious single solution, is the sample-to-sample variability inherent in manual transfer processes that are highly dependent on the skills of the operator. This variability hinders not only the comparison of samples made in different laboratories, but even those originating from the same laboratory, made by a different researcher or at a different time. The development of robotic approaches involving computer vision and machine learning algorithms to identify, pick up, and transfer materials autonomously is therefore an urgent future avenue to be implemented, particularly for research directed toward complex heterostructure architectures. With these future developments, van der Waals heterostructures can offer vast flexibility in the damage-free integration of distinct materials beyond the limits of traditional chemical integration, hence defining a versatile materials platform for exploring electronic and spin interactions across tunable heterostructure interfaces.

Current bottom-up synthesis techniques, as presented in this Primer, are capable of producing vertical stacks for limited sets of materials, lateral heterostructures and superlattices with some degree of control over domain size, spacing and junction quality, as well as more complex architectures of few-layer and multilayer van der Waals crystals, including twisted stacks. The synthesis of vertical van der Waals stacks faces limitations due to materials compatibility and alloying at high growth temperatures; approaches that yield non-equilibrium stacking or interlayer twist are still in their infancy. Lateral heterostructures of increasing complexity, such as those with control over positioning and size of the components (down to the nanometer scale,

where confinement and zone-folding effects become prominent), are attractive because they represent an avenue toward truly 2D monolithic integrated circuits. Future commercial applications depend on further developments in CVD and other synthesis methods. For instance, high-quality 2D semiconductors are still difficult to synthesize over large areas, and the required high synthesis temperatures limit the choice of substrates. Approaches using gaseous precursors, such as metal-organic CVD, are promising for continuous growth of heterostructures without cross-contamination or depletion of powder sources but there are limited precursors that are often hazardous. Heterostructures of metallic and semiconducting components are another future focus towards creating ohmic contacts, interconnects and ultimately integrated circuits.[184] For vertical van der Waals stacks, a recent approach used a focused laser to create a periodic pattern of defects on a semiconducting TMD acting as nucleation centers for the subsequent growth of a metallic component.[65] Such vertical metal-semiconductor contacts create high-performance devices and point to the possibility of using vertically connected 2D metals for highly integrated 2D circuitry. For lateral heterostructures, phase patterning of (ohmic) hetero-phase junctions[58] is attractive for creating multifunctional circuitry due to the inherent chemical and structural compatibility of the metallic and semiconducting components.

Beyond bilayer or few-layer van der Waals heterostructures, high-order van der Waals superlattices could host additional intriguing physics. For example, recent theories predicted that constructing a quasi-3D superlattice could overcome the Mermin-Wagner theorem on magnetism in 2D systems[185] and TMD superlattices with large interlayer exciton binding energy may realize Bose-Einstein condensation at room temperature.[186] It has been challenging to produce superlattices of van der Waals layers by mechanical stacking, but other preparation strategies including CVD growth, intercalation, as well as assembly and roll-up methods[187-189] hold promise for fabricating ideal high-order system for fundamental studies.

Progress in both top-down assembly and bottom-up synthesis, as well as hybrid approaches that combine mechanical stacking, lithographic or laser patterning and vertical or lateral (edge) growth, promises future heterostructures with unprecedented complexity and functionality. Built from both 2D materials and thin films of 3D crystals, such structures can provide access to tunable electronic structure, correlated electron phenomena, diverse types of ordering and spontaneous polarization, such as magnetism,[190] ferroelectricity,[191] charge and spin density waves.[192] These structures can also manipulate light-matter interactions, optical excitations and condensates, with the advantage of facile tuning by electrostatic gating, functional substrate patterns, strain and other external stimuli. A key direction for the future will be the predictive design of new materials with targeted properties by van der Waals integration of different 2D and 3D materials with tailored number of layers, layer sequence and choice of materials. In this way, van der Waals heterostructures promise transformative advances across diverse areas ranging from energy efficient electronics and optoelectronics to emerging quantum information processing.

Glossary Terms

Quantum well: Layer with locally reduced confining potential for electrons and/or holes, sandwiched between barrier layers with higher potential energy for the charge carriers.

Epitaxial heterostructure: Integrated dissimilar 3D crystalline (non-layered) materials with the same or a similar crystal structure and low lattice mismatch, usually formed via crystal growth or

deposition processes, where the crystal orientation of each subsequent component is dictated by the underlying lattice.

Exfoliation: Isolation of a two-dimensional or few-layer flake by peeling of one or more layers from a layered bulk crystal, often involving an adhesive tape whose interaction with the topmost layers of the crystal is stronger than the interlayer interaction.

Micromechanical assembly: Process of stacking of two-dimensional flakes, where the relative position and orientation is precisely controlled by suitable manipulators such as micrometer- or piezo-stages.

Spin-coating: A process for coating flat substrates with thin films, involving the application of a small drop of the liquid coating solution in the center of the substrate followed by the uniform spreading of the material by spinning of the substrate at high rotation frequency.

Axial twisting: Twisting of a ribbon-like 2D or layered crystal around its symmetry axis, continuously changing its orientation and thereby shaping it into the third dimension.

Eshelby twist: Crystal rotation in thin whiskers or nanowires due to a torque between their ends, induced by a screw dislocation (a linear lattice defect) along their symmetry axis.

Moiré potential: A periodic modulation of the local potential by a moiré pattern, notably the twist moiré in twisted van der Waals stacks.

Dirac cone: Cone-shaped, linearly dispersing low-energy valence and conduction bands that meet at a single point at/near the Fermi level, found in graphene and related materials.

Figures and figure legends

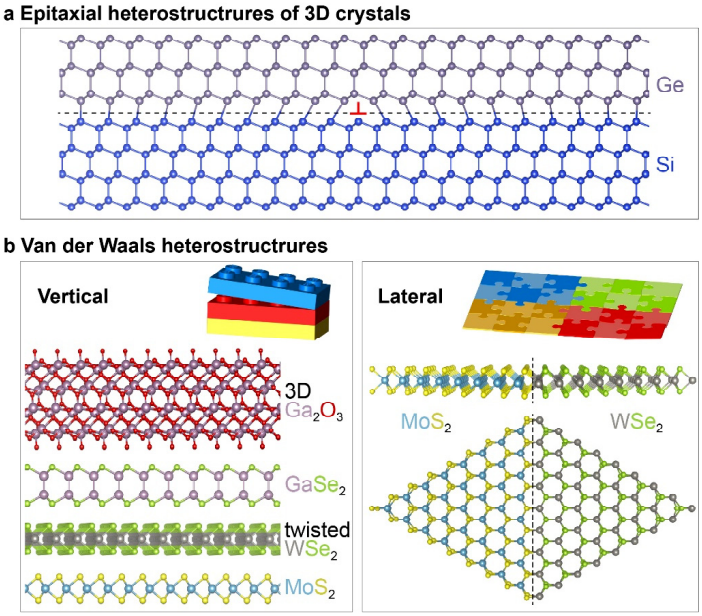

Figure 1. Epitaxial heterostructures of 3D crystals and van der Waals heterostructures. a. Epitaxial heterostructure integrating the isostructural 3D crystals germanium and silicon. The 4.2% lattice mismatch is initially accommodated by elastic strain in the crystals, followed by plastic relaxation through introduction of interfacial misfit dislocations. **b.** Van der Waals heterostructures. Vertical heterostructures involve stacking of sheets held together by van der Waals forces, which provides the highest flexibility in integrating 2D and 3D crystals regardless of structure, lattice mismatch and composition. Lateral heterostructures are a low-dimensional equivalent of epitaxial heterostructures, characterized by covalent bonding at in-plane line interfaces. Lattice mismatch is accommodated by new mechanisms such as out-of-plane deformation, as well as introduction of dislocations.

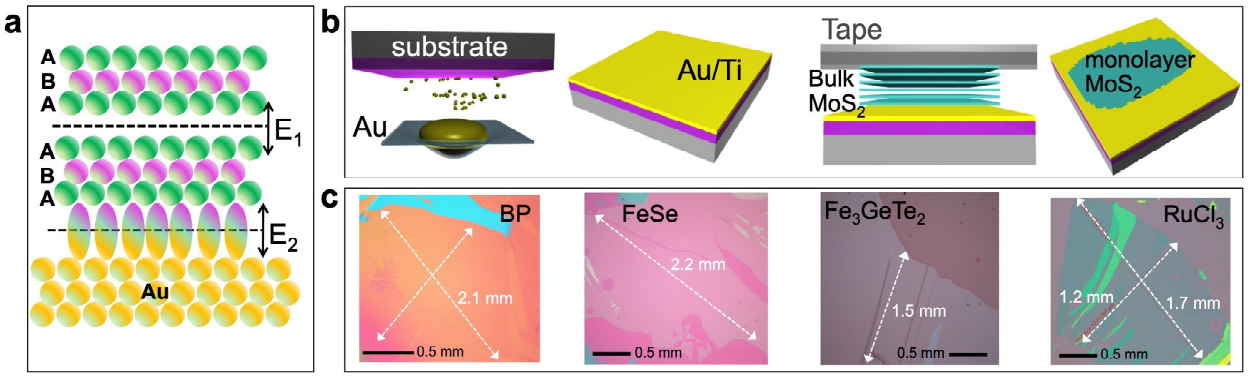

Figure 2. Working principle of Au-film assisted exfoliation and examples of exfoliated 2D crystals. a. Schematic of the interaction mechanism between a layered crystal and gold. Once the substrate interaction exceeds the interlayer interaction, large monolayer flakes can be reliably exfoliated. **b.** Schematic of the gold-film-assisted exfoliation process. **c.** Optical images of large exfoliated 2D crystals.

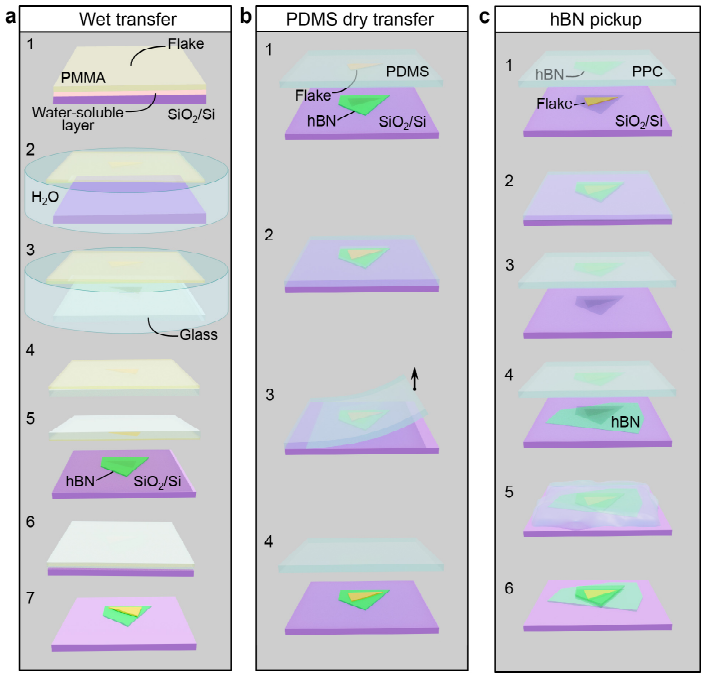

Figure 3. Main steps of different processes for assembly of Van der Waals stacks. a. Wet transfer using a water-soluble polymer/ poly(methyl methacrylate) (PMMA) sandwich. **b.** Deterministic dry transfer using viscoelastic polydimethylsiloxane (PDMS). **c.** Hexagonal boron nitride (h-BN) pick-up.

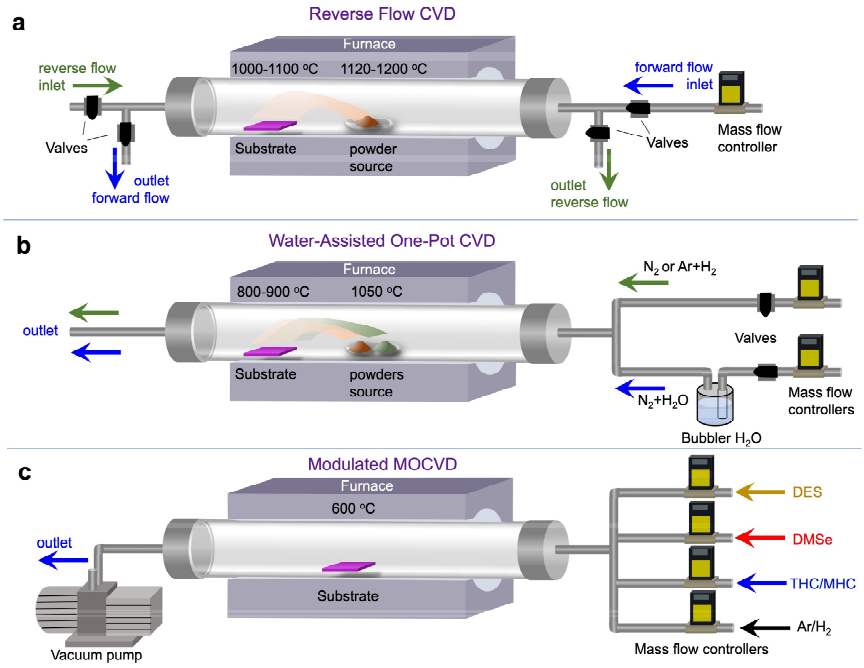

Figure 4. Chemical vapor deposition (CVD) approaches for producing multi-junction heterostructures and superlattices. a. CVD with reverse gas flow to prevent undesired nucleation during heating and cooling.[53] **b.** Water-assisted one-pot CVD allowing continuous production of lateral transition metal dichalcogenides (TMD)-based superlattices by simply switching the composition of the carrier gas.[46,47] **c.** Modulated metal-organic CVD allowing fine control and reproducibility of lateral domains in 2D superlattices.[52]

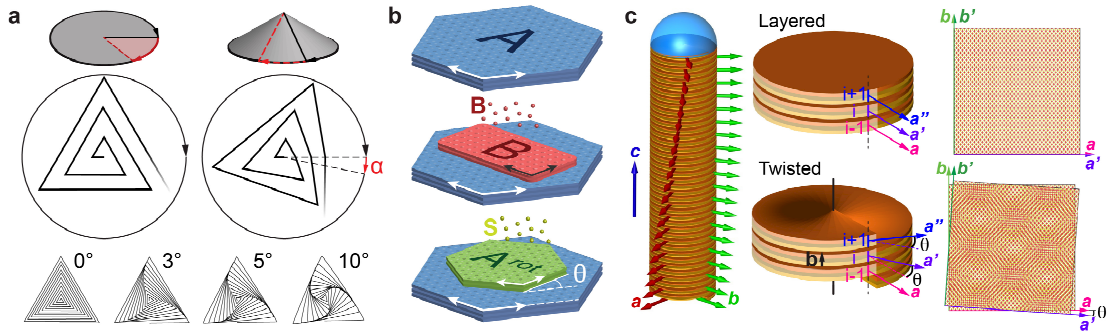

Figure 5.

Bottom-up synthesis approaches with control over interlayer twist. a. Growth spirals on non-Euclidean surfaces, allowing the twist between adjacent layers to be selected via the shape of the non-planar substrate. **b.** Twisted van der Waals epitaxy, in which the final layered crystal phase ($\mathbf{A}^{rot}$) inherits its orientation from a sacrificial intermediate (**B**) rather than the substrate.[96] **c.** Twisted van der Waals nanowires, in which Eshelby twist due to an axial screw dislocation gives rise to an interlayer twist θ and associated twist moiré between adjacent turns of the helicoid crystal. Part **a**. adapted with permission from Ref. [95], part **c.** adapted with permission from Ref. [100].

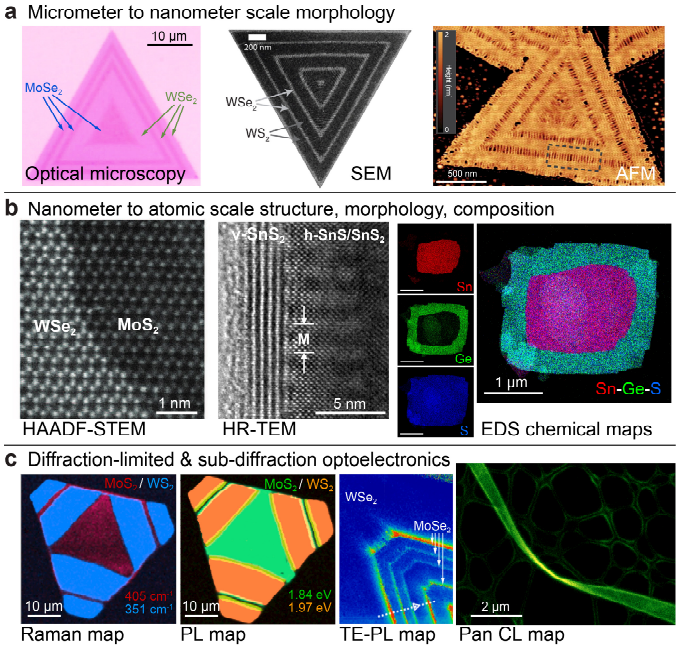

Figure 6. Characterization of van der Waals heterostructures. a. Micrometer to nanometer scale morphology: aa. Optical microscopy ($MoSe_2$-WSe_2 multi-junction lateral heterostructure, adapted from Ref. [46]); ab. Scanning electron microscopy (SEM; WSe_2-WS_2 lateral superlative, adapted from Ref. [52]); atomic force microscopy (AFM; lateral transition metal dichalcogenides TMD superlattice, adapted from Ref. [52]) **b. Nanometer to atomic scale structure, morphology, and composition:** Atomic resolution HAADF-STEM (interface in a 2D lateral heterostructure, adapted from Ref. [51]); High-resolution transmission electron microscopy (HRTEM; interface of a layered wrap-around heterostructure with standing SnS_2 shell and SnS core, adapted from Ref. [75]); energy dispersive spectroscopy (EDS) chemical maps (multilayer SnS-GeS lateral heterostructure, adapted from Ref. [80]) **c. Diffraction-limited and sub-diffraction optoelectronics:** Optical image, composite Raman map and photoluminescence (PL) maps (MoS_2-WS_2 multi-junction lateral heterostructure, adapted from Ref. [46]); tip-enhanced photoluminescence (TE-PL) map ($MoSe_2$-WSe_2 superlattice, adapted from Ref. [114]); Panchromatic cathodoluminescence (CL) map (3D axially twisted van der Waals ribbon, adapted from Ref. [81]).

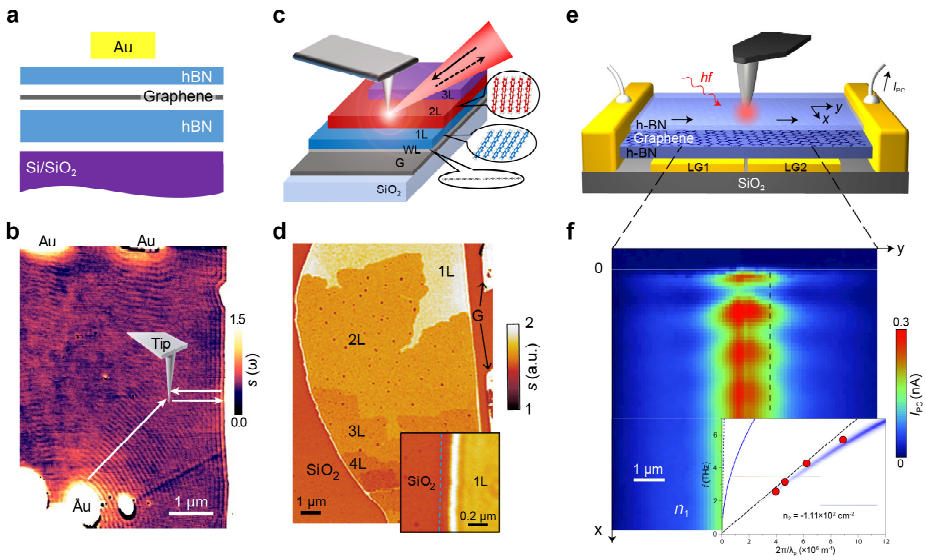

Figure 7. Plasmonic response of graphene based van der Waals heterostructures. a. h-BN/graphene/h-BN heterostructure on a Si/SiO_2 substrate. **b**. Scattering scanning near-field optical microscopy (s-SNOM) imaging of plasmons in the h-BN/graphene/h-BN heterostructure. **c**. Illustration of a pentacene/graphene heterostructure under the s-SNOM probe. **d**. s-SNOM imaging of a pentacene/graphene stack. Inset: zoomed-in view of the sample edge. 'G' marks bare graphene, and '1L' to '5L' represent N-layer pentacene on graphene. **e**. Graphene/h-BN/metal device under s-SNOM. **f**. Photocurrent nanoimaging of the graphene/h-BN/metal device. Inset: dispersion of acoustic plasmons. Panels **a.** and **b.** adapted from Ref. [131]. Panels **c.** and **d.** adapted with permission from Ref. [134]. Panels **e.** and **f.** adapted with permission from Ref. [136].

Box 1| Summary of mechanical stacking methods

PMMA method.[39] The flake is exfoliated onto a PMMA film previously spin coated onto a SiO_2/Si substrate. The PMMA is peeled off the SiO_2/Si and attached to a glass slide. The flake is aligned and transferred to the target substrate using a micromanipulator.

Methyl/n-butyl methacrylate based method (Evalcite method).[193] The flake is exfoliated onto an Evalcite film spin coated onto a glass slide coated with adhesive tape. The flake/Evalcite stack is transferred to a target substrate by gently contacting them and heating to 75-100°C to melt the polymer, which can then be peeled off from the adhesive tape by lifting the glass slide.

Cellulose acetate butyrate based method (Wedging method).[194] The flake is exfoliated onto a SiO_2/Si substrate (hydrophilic); the substrate is dip-coated with a cellulose acetate butyrate copolymer (hydrophobic). Upon immersion, water intercalates (wedges) between the SiO_2 and the copolymer, separating them and stripping off the flake from the SiO_2. The copolymer carrying the flake is then scooped up from the water surface.

PDMS or viscoelastic transfer method.[41,195] The flake is exfoliated onto PDMS and aligned with the target substrate. The flake is transferred by gently contacting the PDMS layer with the target substrate and peeling off very slowly.

PPC or van der Waals pickup method.[42,196-198] The flake is exfoliated onto SiO_2/silicon. A stamp is prepared on a glass slide by coating it with a PDMS layer, followed by spin coating of a thin top layer of PPC (or a similar polymer). The flake is picked up by gently pressing the PPC film against the substrate and lifting up quickly. This process can be modified by first transferring h-BN flakes onto the stamp and using the van der Waals interaction to pick up other 2D flakes from the SiO_2/silicon surface.

References

1 Chen, S. *et al.* Electrically pumped continuous-wave III–V quantum dot lasers on silicon. *Nature Photonics* **10**, 307-311, doi:10.1038/nphoton.2016.21 (2016).

2 Faist, J. *et al.* Quantum Cascade Laser. *Science* **264**, 553-556, doi:doi:10.1126/science.264.5158.553 (1994).

3 Nakamura, S., Mukai, T. & Senoh, M. Candela-class high-brightness InGaN/AlGaN double-heterostructure blue-light-emitting diodes. *Applied Physics Letters* **64**, 1687-1689, doi:10.1063/1.111832 (1994).

4 Jae-Sung, R. *et al.* SiGe heterojunction bipolar transistors and circuits toward terahertz communication applications. *IEEE Transactions on Microwave Theory and Techniques* **52**, 2390-2408, doi:10.1109/TMTT.2004.835984 (2004).

5 Reyren, N. *et al.* Superconducting Interfaces Between Insulating Oxides. *Science* **317**, 1196-1199, doi:doi:10.1126/science.1146006 (2007).

6 Ohtomo, A. & Hwang, H. Y. A high-mobility electron gas at the LaAlO3/SrTiO3 heterointerface. *Nature* **427**, 423-426, doi:10.1038/nature02308 (2004).

7 Fox, M. & Ispasoiu, R. in *Springer Handbook of Electronic and Photonic Materials* (eds Safa Kasap & Peter Capper) 1021-1040 (Springer US, 2007).

8 Pohl, U. W. *Epitaxy of Semiconductors: Introduction to Physical Principles*. (Springer, 2013).

9 Bean, J. C., Feldman, L. C., Fiory, A. T., Nakahara, S. & Robinson, I. K. GexSi1−x/Si strained‐layer superlattice grown by molecular beam epitaxy. *Journal of Vacuum Science & Technology A* **2**, 436-440, doi:10.1116/1.572361 (1984).

10 Mo, Y. W., Savage, D. E., Swartzentruber, B. S. & Lagally, M. G. Kinetic pathway in Stranski-Krastanov growth of Ge on Si(001). *Phys Rev Lett* **65**, 1020-1023, doi:10.1103/PhysRevLett.65.1020 (1990).

11 Hull, R. & Bean, J. C. Nucleation of misfit dislocations in strained‐layer epitaxy in the GexSi1−x/Si system. *Journal of Vacuum Science & Technology A* **7**, 2580-2585, doi:10.1116/1.575800 (1989).

12 Koma, A. Van der Waals epitaxy—a new epitaxial growth method for a highly lattice-mismatched system. *Thin Solid Films* **216**, 72-76, doi:https://doi.org/10.1016/0040-6090(92)90872-9 (1992).

13 Novoselov, K. S. *et al.* Electric Field Effect in Atomically Thin Carbon Films. *Science* **306**, 666-669, doi:doi:10.1126/science.1102896 (2004).

14 Geim, A. K. & Grigorieva, I. V. Van der Waals heterostructures. *Nature* **499**, 419-425, doi:10.1038/nature12385 (2013).

15 Novoselov, K. S., Mishchenko, A., Carvalho, A. & Neto, A. H. C. 2D materials and van der Waals heterostructures. *Science* **353**, aac9439, doi:doi:10.1126/science.aac9439 (2016).

16 Bistritzer, R. & MacDonald, A. H. Moire bands in twisted double-layer graphene. *P Natl Acad Sci USA* **108**, 12233-12237, doi:10.1073/pnas.1108174108 (2011).

17 Levendorf, M. P. *et al.* Graphene and boron nitride lateral heterostructures for atomically thin circuitry. *Nature* **488**, 627-632, doi:10.1038/nature11408 (2012).

18 Sutter, P., Cortes, R., Lahiri, J. & Sutter, E. Interface Formation in Monolayer Graphene-Boron Nitride Heterostructures. *Nano Lett* **12**, 4869-4874, doi:10.1021/nl302398m (2012).

19 Zhang, Y. B., Tan, Y. W., Stormer, H. L. & Kim, P. Experimental observation of the quantum Hall effect and Berry's phase in graphene. *Nature* **438**, 201-204, doi:10.1038/nature04235 (2005).

20 Mak, K. F., Lee, C., Hone, J., Shan, J. & Heinz, T. F. Atomically Thin MoS2: A New Direct-Gap Semiconductor. *Phys Rev Lett* **105**, 136805, doi:10.1103/Physrevlett.105.136805 (2010).
21 Radisavljevic, B., Radenovic, A., Brivio, J., Giacometti, V. & Kis, A. Single-layer MoS2 transistors. *Nat Nanotechnol* **6**, 147-150, doi:10.1038/Nnano.2010.279 (2011).
22 Zhao, W. J. *et al.* Evolution of Electronic Structure in Atomically Thin Sheets of WS2 and WSe2. *ACS Nano* **7**, 791-797, doi:10.1021/nn305275h (2013).
23 Meng, L. *et al.* Buckled Silicene Formation on Ir(111). *Nano Lett* **13**, 685-690, doi:10.1021/nl304347w (2013).
24 Hao, Y. F. *et al.* Oxygen-activated growth and bandgap tunability of large single-crystal bilayer graphene. *Nat Nanotechnol* **11**, 426-431, doi:10.1038/nnano.2015.322 (2016).
25 Sutter, P. W., Flege, J. I. & Sutter, E. A. Epitaxial graphene on ruthenium. *Nat Mater* **7**, 406-411, doi:10.1038/nmat2166 (2008).
26 Chang, C. *et al.* Recent Progress on Two-Dimensional Materials. *Acta Physico-Chimica Sinica* **37**, 2108017 (2021).
27 Huang, Y. *et al.* Reliable Exfoliation of Large-Area High-Quality Flakes of Graphene and Other Two-Dimensional Materials. *ACS Nano* **9**, 10612-10620, doi:10.1021/acsnano.5b04258 (2015).
28 Huang, Y. *et al.* Raman Spectral Band Oscillations in Large Graphene Bubbles. *Phys Rev Lett* **120**, doi:10.1103/Physrevlett.120.186104 (2018).
29 Magda, G. Z. *et al.* Exfoliation of large-area transition metal chalcogenide single layers. *Sci Rep* **5**, 14714, doi:10.1038/Srep14714 (2015).
30 Desai, S. B. *et al.* Gold-Mediated Exfoliation of Ultralarge Optoelectronically-Perfect Monolayers. *Adv Mater* **28**, 4053-4058, doi:10.1002/adma.201506171 (2016).
31 Velicky, M. *et al.* Mechanism of Gold-Assisted Exfoliation of Centimeter-Sized Transition-Metal Dichalcogenide Monolayers. *ACS Nano* **12**, 10463-10472, doi:10.1021/acsnano.8b06101 (2018).
32 Deng, Y. *et al.* Gate-tunable room-temperature ferromagnetism in two-dimensional Fe3GeTe2. *Nature* **563**, 94-99, doi:10.1038/s41586-018-0626-9 (2018).
33 Huang, Y. *et al.* Universal mechanical exfoliation of large-area 2D crystals. *Nat Commun* **11**, 2453, doi:10.1038/s41467-020-16266-w (2020).
34 Huang, Y. *et al.* An efficient route to prepare suspended monolayer for feasible optical and electronic. *InfoMat*, doi:10.1002/inf2.12274 (2021).
35 Liu, F. *et al.* Disassembling 2D van der Waals crystals into macroscopic monolayers and reassembling into artificial lattices. *Science* **367**, 903-906, doi:doi:10.1126/science.aba1416 (2020).
36 Frisenda, R. *et al.* Recent progress in the assembly of nanodevices and van der Waals heterostructures by deterministic placement of 2D materials. *Chemical Society Reviews* **47**, 53-68, doi:10.1039/C7CS00556C (2018).
37 Zhao, Q., Wang, T., Ryu, Y. K., Frisenda, R. & Castellanos-Gomez, A. An inexpensive system for the deterministic transfer of 2D materials. *Journal of Physics: Materials* **3**, 016001, doi:10.1088/2515-7639/ab6a72 (2020).
38 Gant, P. *et al.* A system for the deterministic transfer of 2D materials under inert environmental conditions. *2D Mater* **7**, 025034, doi:10.1088/2053-1583/ab72d6 (2020).
39 Dean, C. R. *et al.* Boron nitride substrates for high-quality graphene electronics. *Nat Nanotechnol* **5**, 722-726, doi:10.1038/nnano.2010.172 (2010).

40 Taychatanapat, T., Watanabe, K., Taniguchi, T. & Jarillo-Herrero, P. Quantum Hall effect and Landau-level crossing of Dirac fermions in trilayer graphene. *Nat Phys* **7**, 621-625, doi:10.1038/nphys2008 (2011).
41 Castellanos-Gomez, A. *et al.* Deterministic transfer of two-dimensional materials by all-dry viscoelastic stamping. *2D Mater* **1**, 011002, doi:10.1088/2053-1583/1/1/011002 (2014).
42 Wang, L. *et al.* One-Dimensional Electrical Contact to a Two-Dimensional Material. *Science* **342**, 614-617, doi:doi:10.1126/science.1244358 (2013).
43 Sutter, P., Huang, Y. & Sutter, E. Nanoscale Integration of Two-Dimensional Materials by Lateral Heteroepitaxy. *Nano Lett* **14**, 4846-4851, doi:10.1021/nl502110q (2014).
44 Lee, J. *et al.* Direct Epitaxial Synthesis of Selective Two-Dimensional Lateral Heterostructures. *ACS Nano* **13**, 13047-13055, doi:10.1021/acsnano.9b05722 (2019).
45 Gong, Y. J. *et al.* Two-Step Growth of Two-Dimensional WSe2/MoSe2 Heterostructures. *Nano Lett* **15**, 6135-6141, doi:10.1021/acs.nanolett.5b02423 (2015).
46 Sahoo, P. K., Memaran, S., Xin, Y., Balicas, L. & Gutierrez, H. R. One-pot growth of two-dimensional lateral heterostructures via sequential edge-epitaxy. *Nature* **553**, 63-67 (2018).
47 Sahoo, P. K. *et al.* Bilayer Lateral Heterostructures of Transition-Metal Dichalcogenides and Their Optoelectronic Response. *ACS Nano* **13**, 12372-12384, doi:10.1021/acsnano.9b04957 (2019).
48 Gong, Y. J. *et al.* Vertical and in-plane heterostructures from WS2/MoS2 monolayers. *Nat Mater* **13**, 1135-1142, doi:10.1038/Nmat4091 (2014).
49 Huang, C. M. *et al.* Lateral heterojunctions within monolayer MoSe2-WSe2 semiconductors. *Nat Mater* **13**, 1096-1101, doi:10.1038/Nmat4064 (2014).
50 Duan, X. D. *et al.* Lateral epitaxial growth of two-dimensional layered semiconductor heterojunctions. *Nat Nanotechnol* **9**, 1024-1030, doi:10.1038/Nnano.2014.222 (2014).
51 Li, M. Y. *et al.* Epitaxial growth of a monolayer WSe2-MoS2 lateral p-n junction with an atomically sharp interface. *Science* **349**, 524-528, doi:10.1126/science.aab4097 (2015).
52 Xie, S. E. *et al.* Coherent, atomically thin transition-metal dichalcogenide superlattices with engineered strain. *Science* **359**, 1131-1135, doi:10.1126/science.aao5360 (2018).
53 Zhang, Z. W. *et al.* Robust epitaxial growth of two-dimensional heterostructures, multiheterostructures, and superlattices. *Science* **357**, 788-792, doi:DOI 10.1126/science.aan6814 (2017).
54 Mahjouri-Samani, M. *et al.* Patterned arrays of lateral heterojunctions within monolayer two-dimensional semiconductors. *Nat Commun* **6**, 7749, doi:10.1038/ncomms8749 (2015).
55 Taghinejad, H. *et al.* Synthetic Engineering of Morphology and Electronic Band Gap in Lateral Heterostructures of Monolayer Transition Metal Dichalcogenides. *ACS Nano* **14**, 6323-6330, doi:10.1021/acsnano.0c02885 (2020).
56 Li, H. N. *et al.* Laterally Stitched Heterostructures of Transition Metal Dichalcogenide: Chemical Vapor Deposition Growth on Lithographically Patterned Area. *ACS Nano* **10**, 10516-10523, doi:10.1021/acsnano.6b06496 (2016).
57 Afaneh, T., Sahoo, P. K., Nobrega, I. A. P., Xin, Y. & Gutierrez, H. R. Laser-Assisted Chemical Modification of Monolayer Transition Metal Dichalcogenides. *Adv Funct Mater* **28**, 1802949, doi:10.1002/adfm.201802949 (2018).
58 Cho, S. *et al.* Phase patterning for ohmic homojunction contact in MoTe2. *Science* **349**, 625-628, doi:10.1126/science.aab3175 (2015).
59 Sun, L. *et al.* Chemical vapour deposition. *Nat Rev Methods Primers* **1**, 5, doi:https://doi.org/10.1038/s43586-020-00005-y (2021).

60 Li, H. L. *et al.* Lateral Growth of Composition Graded Atomic Layer MoS2(1-x)Se2x Nanosheets. *J Am Chem Soc* **137**, 5284-5287, doi:10.1021/jacs.5b01594 (2015).
61 Wu, X. P. *et al.* Spatially composition-modulated two-dimensional WS2xSe2(1-x) nanosheets. *Nanoscale* **9**, 4707-4712, doi:10.1039/c7nr00272f (2017).
62 Yu, H. *et al.* Spatially Graded Millimeter Sized Mo1-xWxS2 Monolayer Alloys: Synthesis and Memory Effect. *ACS Appl Mater Interf* **13**, 44693-44702, doi:10.1021/acsami.1c09176 (2021).
63 Nugera, F. A. *et al.* Bandgap Engineering in 2D Lateral Heterostructures of Transition Metal Dichalcogenides via Controlled Alloying. *Small* **18**, 2106600, doi:https://doi.org/10.1002/smll.202106600 (2022).
64 Yang, T. *et al.* Van der Waals epitaxial growth and optoelectronics of large-scale WSe2/SnS2 vertical bilayer p–n junctions. *Nat Commun* **8**, 1906, doi:10.1038/s41467-017-02093-z (2017).
65 Li, J. *et al.* General synthesis of two-dimensional van der Waals heterostructure arrays. *Nature* **579**, 368-374, doi:10.1038/s41586-020-2098-y (2020).
66 Bergeron, H., Lebedev, D. & Hersam, M. C. Polymorphism in Post-Dichalcogenide Two-Dimensional Materials. *Chemical Reviews* **121**, 2713-2775, doi:10.1021/acs.chemrev.0c00933 (2021).
67 Huang, Y. *et al.* Tin Disulfide—An Emerging Layered Metal Dichalcogenide Semiconductor: Materials Properties and Device Characteristics. *ACS Nano* **8**, 10743-10755, doi:10.1021/nn504481r (2014).
68 Yu, J. *et al.* Monodisperse SnS2 Nanosheets for High-Performance Photocatalytic Hydrogen Generation. *ACS Appl Mater Interf* **6**, 22370-22377, doi:10.1021/am506396z (2014).
69 Tian, Z., Guo, C., Zhao, M., Li, R. & Xue, J. Two-Dimensional SnS: A Phosphorene Analogue with Strong In-Plane Electronic Anisotropy. *ACS Nano* **11**, 2219-2226, doi:10.1021/acsnano.6b08704 (2017).
70 Luan, Y. *et al.* Imaging Anisotropic Waveguide Exciton Polaritons in Tin Sulfide. *Nano Lett*, doi:10.1021/acs.nanolett.1c03833 (2022).
71 Lin, S. *et al.* Accessing valley degree of freedom in bulk Tin(II) sulfide at room temperature. *Nat Commun* **9**, 1455, doi:10.1038/s41467-018-03897-3 (2018).
72 Higashitarumizu, N. *et al.* Purely in-plane ferroelectricity in monolayer SnS at room temperature. *Nat Commun* **11**, 2428, doi:10.1038/s41467-020-16291-9 (2020).
73 Sutter, P., Komsa, H. P., Lu, H., Gruverman, A. & Sutter, E. Few-layer tin sulfide (SnS): Controlled synthesis, thickness dependent vibrational properties, and ferroelectricity. *Nano Today* **37**, 101082, doi:https://doi.org/10.1016/j.nantod.2021.101082 (2021).
74 Sutter, E. *et al.* Electron-Beam Induced Transformations of Layered Tin Dichalcogenides. *Nano Lett* **16**, 4410-4416, doi:10.1021/acs.nanolett.6b01541 (2016).
75 Sutter, P., Wang, J. & Sutter, E. Wrap-Around Core–Shell Heterostructures of Layered Crystals. *Adv Mater* **31**, 1902166, doi:https://doi.org/10.1002/adma.201902166 (2019).
76 Sutter, P. & Sutter, E. Growth Mechanisms of Anisotropic Layered Group IV Chalcogenides on van der Waals Substrates for Energy Conversion Applications. *ACS Appl Nano Mater* **1**, 3026-3034, doi:10.1021/acsanm.8b00660 (2018).
77 Sutter, E., Wang, J. & Sutter, P. Surface Passivation by Excess Sulfur for Controlled Synthesis of Large, Thin SnS Flakes. *Chemistry of Materials* **32**, 8034-8042, doi:10.1021/acs.chemmater.0c03297 (2020).

78 Sutter, E., Wang, J. & Sutter, P. Nanoparticle-Templated Thickness Controlled Growth, Thermal Stability, and Decomposition of Ultrathin Tin Sulfide Plates. *Chemistry of Materials* **31**, 2563-2570, doi:10.1021/acs.chemmater.9b00177 (2019).
79 Sutter, E., Wang, J. & Sutter, P. Lateral Heterostructures of Multilayer GeS and SnS van der Waals Crystals. *ACS Nano* **14**, 12248-12255, doi:10.1021/acsnano.0c05978 (2020).
80 Sutter, E., Unocic, R. R., Idrobo, J.-C. & Sutter, P. Multilayer Lateral Heterostructures of Van Der Waals Crystals with Sharp, Carrier–Transparent Interfaces. *Advanced Science* **9**, 2103830, doi:https://doi.org/10.1002/advs.202103830 (2022).
81 Sutter, P., Khorashad, L. K., Argyropoulos, C. & Sutter, E. Cathodoluminescence of Ultrathin Twisted Ge1−xSnxS van der Waals Nanoribbon Waveguides. *Adv Mater* **33**, 2006649, doi:https://doi.org/10.1002/adma.202006649 (2021).
82 Molina-Mendoza, A. J. *et al.* Franckeite as a naturally occurring van der Waals heterostructure. *Nat Commun* **8**, 14409, doi:10.1038/ncomms14409 (2017).
83 Velický, M. *et al.* Exfoliation of natural van der Waals heterostructures to a single unit cell thickness. *Nat Commun* **8**, 14410, doi:10.1038/ncomms14410 (2017).
84 Ray, K. *et al.* Photoresponse of Natural van der Waals Heterostructures. *ACS Nano* **11**, 6024-6030, doi:10.1021/acsnano.7b01918 (2017).
85 Niu, Y. *et al.* Mechanical and liquid phase exfoliation of cylindrite: a natural van der Waals superlattice with intrinsic magnetic interactions. *2D Mater* **6**, 035023, doi:10.1088/2053-1583/ab1a4c (2019).
86 Dasgupta, A., Yang, X. & Gao, J. Naturally occurring van der Waals heterostructure lengenbachite with strong in-plane structural and optical anisotropy. *npj 2D Materials and Applications* **5**, 88, doi:10.1038/s41699-021-00271-8 (2021).
87 Frisenda, R., Niu, Y., Gant, P., Muñoz, M. & Castellanos-Gomez, A. Naturally occurring van der Waals materials. *npj 2D Materials and Applications* **4**, 38, doi:10.1038/s41699-020-00172-2 (2020).
88 Liu, K. *et al.* Evolution of interlayer coupling in twisted molybdenum disulfide bilayers. *Nat Commun* **5**, 4966, doi:10.1038/ncomms5966 (2014).
89 Yeh, P.-C. *et al.* Direct Measurement of the Tunable Electronic Structure of Bilayer MoS2 by Interlayer Twist. *Nano Lett* **16**, 953-959, doi:10.1021/acs.nanolett.5b03883 (2016).
90 Cao, Y. *et al.* Correlated insulator behaviour at half-filling in magic-angle graphene superlattices. *Nature* **556**, 80-84, doi:10.1038/nature26154 (2018).
91 Cao, Y. *et al.* Unconventional superconductivity in magic-angle graphene superlattices. *Nature* **556**, 43-50, doi:10.1038/nature26160 (2018).
92 Kim, K. *et al.* van der Waals Heterostructures with High Accuracy Rotational Alignment. *Nano Lett* **16**, 1989-1995, doi:10.1021/acs.nanolett.5b05263 (2016).
93 Peymanirad, F. *et al.* Thermal activated rotation of graphene flake on graphene. *2D Mater* **4**, 025015, doi:10.1088/2053-1583/aa58a4 (2017).
94 Sun, L. *et al.* Hetero-site nucleation for growing twisted bilayer graphene with a wide range of twist angles. *Nat Commun* **12**, 2391, doi:10.1038/s41467-021-22533-1 (2021).
95 Zhao, Y. *et al.* Supertwisted spirals of layered materials enabled by growth on non-Euclidean surfaces. *Science* **370**, 442-445, doi:doi:10.1126/science.abc4284 (2020).
96 Sutter, P., Ibragimova, R., Komsa, H.-P., Parkinson, B. A. & Sutter, E. Self-organized twist-heterostructures via aligned van der Waals epitaxy and solid-state transformations. *Nat Commun* **10**, 5528, doi:10.1038/s41467-019-13488-5 (2019).

97 Eshelby, J. D. Screw Dislocations in Thin Rods. *Journal of Applied Physics* **24**, 176-179, doi:10.1063/1.1721234 (1953).
98 Sutter, P., Wimer, S. & Sutter, E. Chiral twisted van der Waals nanowires. *Nature* **570**, 354-357, doi:10.1038/s41586-019-1147-x (2019).
99 Sutter, E. & Sutter, P. Ultrathin Twisted Germanium Sulfide van der Waals Nanowires by Bismuth Catalyzed Vapor–Liquid–Solid Growth. *Small* **17**, 2104784, doi:https://doi.org/10.1002/smll.202104784 (2021).
100 Sutter, P., Idrobo, J.-C. & Sutter, E. Van der Waals Nanowires with Continuously Variable Interlayer Twist and Twist Homojunctions. *Adv Funct Mater* **31**, 2006412, doi:https://doi.org/10.1002/adfm.202006412 (2021).
101 Roddaro, S., Pingue, P., Piazza, V., Pellegrini, V. & Beltram, F. The Optical Visibility of Graphene: Interference Colors of Ultrathin Graphite on SiO2. *Nano Lett* **7**, 2707-2710, doi:10.1021/nl0711581 (2007).
102 Jung, I. *et al.* Simple Approach for High-Contrast Optical Imaging and Characterization of Graphene-Based Sheets. *Nano Lett* **7**, 3569-3575, doi:10.1021/nl0714177 (2007).
103 Ni, Z. H. *et al.* Graphene Thickness Determination Using Reflection and Contrast Spectroscopy. *Nano Lett* **7**, 2758-2763, doi:10.1021/nl071254m (2007).
104 Bian, K. *et al.* Scanning probe microscopy. *Nature Reviews Methods Primers* **1**, 36, doi:10.1038/s43586-021-00033-2 (2021).
105 Wang, Z.-J. *et al.* Direct Observation of Graphene Growth and Associated Copper Substrate Dynamics by in Situ Scanning Electron Microscopy. *ACS Nano* **9**, 1506-1519, doi:10.1021/nn5059826 (2015).
106 Sang, X. *et al.* In situ edge engineering in two-dimensional transition metal dichalcogenides. *Nature Communications* **9**, 2051, doi:10.1038/s41467-018-04435-x (2018).
107 Sutter, P. & Sutter, E. Microscopy of Graphene Growth, Processing, and Properties. *Advanced Functional Materials* **23**, 2617-2634, doi:https://doi.org/10.1002/adfm.201203426 (2013).
108 Sutter, P., Albrecht, P., Tong, X. & Sutter, E. Mechanical Decoupling of Graphene from Ru(0001) by Interfacial Reaction with Oxygen. *The Journal of Physical Chemistry C* **117**, 6320-6324, doi:10.1021/jp400838j (2013).
109 Sutter, P., Hybertsen, M. S., Sadowski, J. T. & Sutter, E. Electronic Structure of Few-Layer Epitaxial Graphene on Ru(0001). *Nano Lett* **9**, 2654-2660, doi:10.1021/nl901040v (2009).
110 Jin, W. *et al.* Direct Measurement of the Thickness-Dependent Electronic Band Structure of MoS2 Using Angle-Resolved Photoemission Spectroscopy. *Phys Rev Lett* **111**, 106801, doi:10.1103/PhysRevLett.111.106801 (2013).
111 Fei, Z. *et al.* Gate-tuning of graphene plasmons revealed by infrared nano-imaging. *Nature* **487**, 82-85, doi:10.1038/nature11253 (2012).
112 Iranzo, D. A. *et al.* Probing the ultimate plasmon confinement limits with a van der Waals heterostructure. *Science* **360**, 291-295, doi:doi:10.1126/science.aar8438 (2018).
113 Sunku, S. S. *et al.* Photonic crystals for nano-light in moiré graphene superlattices. *Science* **362**, 1153-1156, doi:doi:10.1126/science.aau5144 (2018).
114 Sahoo, P. K. *et al.* Probing nano-heterogeneity and aging effects in lateral 2D heterostructures using tip-enhanced photoluminescence. *Opt Mater Express* **9**, 1620-1631, doi:10.1364/Ome.9.001620 (2019).

115 Sutter, E., Zhang, B., Sun, M. & Sutter, P. Few-Layer to Multilayer Germanium(II) Sulfide: Synthesis, Structure, Stability, and Optoelectronics. *ACS Nano* **13**, 9352-9362, doi:10.1021/acsnano.9b03986 (2019).
116 Sutter, P., Argyropoulos, C. & Sutter, E. Germanium Sulfide Nano-Optics Probed by STEM-Cathodoluminescence Spectroscopy. *Nano Lett* **18**, 4576-4583, doi:10.1021/acs.nanolett.8b01840 (2018).
117 Sutter, E., French, J. S., Sutter, S., Idrobo, J. C. & Sutter, P. Vapor–Liquid–Solid Growth and Optoelectronics of Gallium Sulfide van der Waals Nanowires. *ACS Nano* **14**, 6117-6126, doi:10.1021/acsnano.0c01919 (2020).
118 Sutter, P., French, J. S., Khosravi Khorashad, L., Argyropoulos, C. & Sutter, E. Optoelectronics and Nanophotonics of Vapor–Liquid–Solid Grown GaSe van der Waals Nanoribbons. *Nano Lett* **21**, 4335-4342, doi:10.1021/acs.nanolett.1c00891 (2021).
119 Furchi, M. M., Pospischil, A., Libisch, F., Burgdörfer, J. & Mueller, T. Photovoltaic Effect in an Electrically Tunable van der Waals Heterojunction. *Nano Lett* **14**, 4785-4791, doi:10.1021/nl501962c (2014).
120 Lee, C.-H. *et al.* Atomically thin p–n junctions with van der Waals heterointerfaces. *Nat Nanotechnol* **9**, 676-681, doi:10.1038/nnano.2014.150 (2014).
121 Cheng, R. *et al.* Electroluminescence and Photocurrent Generation from Atomically Sharp WSe2/MoS2 Heterojunction p–n Diodes. *Nano Lett* **14**, 5590-5597, doi:10.1021/nl502075n (2014).
122 Withers, F. *et al.* Light-emitting diodes by band-structure engineering in van der Waals heterostructures. *Nat Mater* **14**, 301-306, doi:10.1038/nmat4205 (2015).
123 Zhang, N. *et al.* Moiré Intralayer Excitons in a MoSe2/MoS2 Heterostructure. *Nano Lett* **18**, 7651-7657, doi:10.1021/acs.nanolett.8b03266 (2018).
124 Rivera, P. *et al.* Interlayer valley excitons in heterobilayers of transition metal dichalcogenides. *Nat Nanotechnol* **13**, 1004-1015, doi:10.1038/s41565-018-0193-0 (2018).
125 Kunstmann, J. *et al.* Momentum-space indirect interlayer excitons in transition-metal dichalcogenide van der Waals heterostructures. *Nat Phys* **14**, 801-805, doi:10.1038/s41567-018-0123-y (2018).
126 Tran, K. *et al.* Evidence for moire excitons in van der Waals heterostructures. *Nature* **567**, 71-75, doi:10.1038/s41586-019-0975-z (2019).
127 Seyler, K. L. *et al.* Signatures of moire-trapped valley excitons in MoSe2/WSe2 heterobilayers. *Nature* **567**, 66-70, doi:10.1038/s41586-019-0957-1 (2019).
128 Alexeev, E. M. *et al.* Resonantly hybridized excitons in moire superlattices in van der Waals heterostructures. *Nature* **572**, 81-86, doi:10.1038/s41586-019-1412-z (2019).
129 Chen, J. *et al.* Optical nano-imaging of gate-tunable graphene plasmons. *Nature* **487**, 77-81, doi:10.1038/nature11254 (2012).
130 Woessner, A. *et al.* Highly confined low-loss plasmons in graphene–boron nitride heterostructures. *Nat Mater* **14**, 421-425, doi:10.1038/nmat4169 (2015).
131 Ni, G. X. *et al.* Fundamental limits to graphene plasmonics. *Nature* **557**, 530-533, doi:10.1038/s41586-018-0136-9 (2018).
132 Bandurin, D. A. *et al.* Resonant terahertz detection using graphene plasmons. *Nat Commun* **9**, 5392, doi:10.1038/s41467-018-07848-w (2018).
133 Ni, G. X. *et al.* Plasmons in graphene moiré superlattices. *Nat Mater* **14**, 1217-1222, doi:10.1038/nmat4425 (2015).

134 Hu, F. *et al.* Tailored Plasmons in Pentacene/Graphene Heterostructures with Interlayer Electron Transfer. *Nano Lett* **19**, 6058-6064, doi:10.1021/acs.nanolett.9b01945 (2019).
135 Rizzo, D. J. *et al.* Charge-Transfer Plasmon Polaritons at Graphene/α-RuCl3 Interfaces. *Nano Lett* **20**, 8438-8445, doi:10.1021/acs.nanolett.0c03466 (2020).
136 Alonso-González, P. *et al.* Acoustic terahertz graphene plasmons revealed by photocurrent nanoscopy. *Nat Nanotechnol* **12**, 31-35, doi:10.1038/nnano.2016.185 (2017).
137 Lee, I.-H., Yoo, D., Avouris, P., Low, T. & Oh, S.-H. Graphene acoustic plasmon resonator for ultrasensitive infrared spectroscopy. *Nat Nanotechnol* **14**, 313-319, doi:10.1038/s41565-019-0363-8 (2019).
138 Liu, Y., Huang, Y. & Duan, X. Van der Waals integration before and beyond two-dimensional materials. *Nature* **567**, 323-333, doi:10.1038/s41586-019-1013-x (2019).
139 Wang, P. & Duan, X. Probing and pushing the limit of emerging electronic materials via van der Waals integration. *MRS Bulletin* **46**, 534-546, doi:10.1557/s43577-021-00130-3 (2021).
140 Cheng, R. *et al.* High-frequency self-aligned graphene transistors with transferred gate stacks. *Proceedings of the National Academy of Sciences* **109**, 11588-11592, doi:10.1073/pnas.1205696109 (2012).
141 Liu, Y. *et al.* Approaching the Schottky–Mott limit in van der Waals metal–semiconductor junctions. *Nature* **557**, 696-700, doi:10.1038/s41586-018-0129-8 (2018).
142 Wang, C. *et al.* Monolayer atomic crystal molecular superlattices. *Nature* **555**, 231-236, doi:10.1038/nature25774 (2018).
143 Liao, L. *et al.* High-κ oxide nanoribbons as gate dielectrics for high mobility top-gated graphene transistors. *Proceedings of the National Academy of Sciences* **107**, 6711-6715, doi:10.1073/pnas.0914117107 (2010).
144 Liao, L. *et al.* High-speed graphene transistors with a self-aligned nanowire gate. *Nature* **467**, 305-308, doi:10.1038/nature09405 (2010).
145 Liao, L. *et al.* High-Performance Top-Gated Graphene-Nanoribbon Transistors Using Zirconium Oxide Nanowires as High-Dielectric-Constant Gate Dielectrics. *Adv Mater* **22**, 1941-1945, doi:https://doi.org/10.1002/adma.200904415 (2010).
146 Cheng, R. *et al.* Few-layer molybdenum disulfide transistors and circuits for high-speed flexible electronics. *Nat Commun* **5**, 5143, doi:10.1038/ncomms6143 (2014).
147 Lee, S.-J. *et al.* Programmable devices based on reversible solid-state doping of two-dimensional semiconductors with superionic silver iodide. *Nature Electronics* **3**, 630-637, doi:10.1038/s41928-020-00472-x (2020).
148 Tung, R. T. The physics and chemistry of the Schottky barrier height. *Applied Physics Reviews* **1**, 011304, doi:10.1063/1.4858400 (2014).
149 Chen, P. *et al.* Approaching the intrinsic exciton physics limit in two-dimensional semiconductor diodes. *Nature* **599**, 404-410, doi:10.1038/s41586-021-03949-7 (2021).
150 Haick, H., Ambrico, M., Ghabboun, J., Ligonzo, T. & Cahen, D. Contacting organic molecules by metal evaporation. *Physical Chemistry Chemical Physics* **6**, 4538-4541, doi:10.1039/B411490F (2004).
151 Wang, Y. *et al.* Probing photoelectrical transport in lead halide perovskites with van der Waals contacts. *Nat Nanotechnol* **15**, 768-775, doi:10.1038/s41565-020-0729-y (2020).
152 Liu, Y. *et al.* van der Waals Integrated Devices Based on Nanomembranes of 3D Materials. *Nano Lett* **20**, 1410-1416, doi:10.1021/acs.nanolett.9b05027 (2020).

153 Sutter, P., Zahl, P. & Sutter, E. Continuous formation and faceting of SiGe islands on Si(100). *Applied Physics Letters* **82**, 3454-3456, doi:10.1063/1.1577386 (2003).
154 Zhou, J. *et al.* Layered Intercalation Materials. *Adv Mater* **33**, 2004557, doi:https://doi.org/10.1002/adma.202004557 (2021).
155 Yankowitz, M. *et al.* Emergence of superlattice Dirac points in graphene on hexagonal boron nitride. *Nat Phys* **8**, 382-386, doi:10.1038/Nphys2272 (2012).
156 Dean, C. R. *et al.* Hofstadter's butterfly and the fractal quantum Hall effect in moire superlattices. *Nature* **497**, 598-602, doi:10.1038/nature12186 (2013).
157 Yang, W. *et al.* Epitaxial growth of single-domain graphene on hexagonal boron nitride. *Nat Mater* **12**, 792-797, doi:10.1038/NMAT3695 (2013).
158 Hunt, B. *et al.* Massive Dirac Fermions and Hofstadter Butterfly in a van der Waals Heterostructure. *Science* **340**, 1427-1430, doi:10.1126/science.1237240 (2013).
159 Yang, W. *et al.* Hofstadter Butterfly and Many-Body Effects in Epitaxial Graphene Superlattice. *Nano Lett* **16**, 2387-2392, doi:10.1021/acs.nanolett.5b05161 (2016).
160 Chen, G. *et al.* Evidence of a gate-tunable Mott insulator in a trilayer graphene moiré superlattice. *Nat Phys* **15**, 237-241, doi:10.1038/s41567-018-0387-2 (2019).
161 Wang, L. *et al.* Evidence for a fractional fractal quantum Hall effect in graphene superlattices. *Science* **350**, 1231-1234, doi:10.1126/science.aad2102 (2015).
162 Wang, D. M. *et al.* Thermally Induced Graphene Rotation on Hexagonal Boron Nitride. *Phys Rev Lett* **116**, doi:10.1103/Physrevlett.116.126101 (2016).
163 Woods, C. R. *et al.* Macroscopic self-reorientation of interacting two-dimensional crystals. *Nat Commun* **7**, doi:10.1038/Ncomms10800 (2016).
164 Yankowitz, M. *et al.* Tuning superconductivity in twisted bilayer graphene. *Science* **363**, 1059-1064, doi:10.1126/science.aav1910 (2019).
165 Liu, X. M. *et al.* Tunable spin-polarized correlated states in twisted double bilayer graphene. *Nature* **583**, 221-225, doi:10.1038/s41586-020-2458-7 (2020).
166 Cao, Y. *et al.* Tunable correlated states and spin-polarized phases in twisted bilayer-bilayer graphene. *Nature* **583**, 215-+, doi:10.1038/s41586-020-2260-6 (2020).
167 Shen, C. *et al.* Correlated states in twisted double bilayer graphene. *Nat Phys* **16**, 520-525, doi:10.1038/s41567-020-0825-9 (2020).
168 He, M. H. *et al.* Symmetry breaking in twisted double bilayer graphene. *Nat Phys* **17**, 26-30, doi:10.1038/s41567-020-1030-6 (2021).
169 Wang, L. *et al.* Correlated electronic phases in twisted bilayer transition metal dichalcogenides. *Nat Mater* **19**, 861-866, doi:10.1038/s41563-020-0708-6 (2020).
170 Regan, E. C. *et al.* Mott and generalized Wigner crystal states in WSe2/WS2 moire superlattices. *Nature* **579**, 359-363, doi:10.1038/s41586-020-2092-4 (2020).
171 Tang, Y. H. *et al.* Simulation of Hubbard model physics in WSe2/WS2 moire superlattices. *Nature* **579**, 353-358, doi:10.1038/s41586-020-2085-3 (2020).
172 Jin, C. H. *et al.* Observation of moire excitons in WSe2/WS2 heterostructure superlattices. *Nature* **567**, 76-80, doi:10.1038/s41586-019-0976-y (2019).
173 Xian, L. D., Kennes, D. M., Tancogne-Dejean, N., Altarelli, M. & Rubio, A. Multiflat Bands and Strong Correlations in Twisted Bilayer Boron Nitride: Doping-Induced Correlated Insulator and Superconductor. *Nano Lett* **19**, 4934-4940, doi:10.1021/acs.nanolett.9b00986 (2019).
174 Kennes, D. M., Xian, L., Claassen, M. & Rubio, A. One-dimensional flat bands in twisted bilayer germanium selenide. *Nat Commun* **11**, doi:10.1038/S41467-020-14947-0 (2020).

175 Kennes, D. M. *et al.* Moire heterostructures as a condensed-matter quantum simulator. *Nat Phys* **17**, 155-163, doi:10.1038/s41567-020-01154-3 (2021).
176 Masubuchi, S. *et al.* Autonomous robotic searching and assembly of two-dimensional crystals to build van der Waals superlattices. *Nat Commun* **9**, 1413, doi:10.1038/s41467-018-03723-w (2018).
177 Frisenda, R. & Castellanos-Gomez, A. Robotic assembly of artificial nanomaterials. *Nat Nanotechnol* **13**, 441-442, doi:10.1038/s41565-018-0156-5 (2018).
178 Tang, L., Tan, J., Nong, H., Liu, B. & Cheng, H.-M. Chemical Vapor Deposition Growth of Two-Dimensional Compound Materials: Controllability, Material Quality, and Growth Mechanism. *Accounts of Materials Research* **2**, 36-47, doi:10.1021/accountsmr.0c00063 (2021).
179 Tang, L. *et al.* Vertical Chemical Vapor Deposition Growth of Highly Uniform 2D Transition Metal Dichalcogenides. *ACS Nano* **14**, 4646-4653, doi:10.1021/acsnano.0c00296 (2020).
180 Kretinin, A. V. *et al.* Electronic Properties of Graphene Encapsulated with Different Two-Dimensional Atomic Crystals. *Nano Lett* **14**, 3270-3276, doi:10.1021/nl5006542 (2014).
181 Haigh, S. J. *et al.* Cross-sectional imaging of individual layers and buried interfaces of graphene-based heterostructures and superlattices. *Nat Mater* **11**, 764-767, doi:10.1038/nmat3386 (2012).
182 Kang, K. *et al.* Layer-by-layer assembly of two-dimensional materials into wafer-scale heterostructures. *Nature* **550**, 229-233, doi:10.1038/nature23905 (2017).
183 Mannix, A. J. *et al.* Robotic four-dimensional pixel assembly of van der Waals solids. *Nat Nanotechnol* **17**, 361-366, doi:10.1038/s41565-021-01061-5 (2022).
184 Zhang, Y. *et al.* Edge-Epitaxial Growth of 2D NbS2-WS2 Lateral Metal-Semiconductor Heterostructures. *Adv Mater* **30**, 1803665, doi:10.1002/adma.201803665 (2018).
185 Mermin, N. D. & Wagner, H. Absence of Ferromagnetism or Antiferromagnetism in One- or Two-Dimensional Isotropic Heisenberg Models. *Phys Rev Lett* **17**, 1133-1136, doi:10.1103/PhysRevLett.17.1133 (1966).
186 Van der Donck, M. *et al.* Three-dimensional electron-hole superfluidity in a superlattice close to room temperature. *Physical Review B* **102**, 060503, doi:10.1103/PhysRevB.102.060503 (2020).
187 Ren, H., Wan, Z. & Duan, X. Van der Waals superlattices. *National Science Review*, doi:10.1093/nsr/nwab166 (2021).
188 Zhao, B. *et al.* High-order superlattices by rolling up van der Waals heterostructures. *Nature* **591**, 385-390, doi:10.1038/s41586-021-03338-0 (2021).
189 Lin, Z. *et al.* High-yield exfoliation of 2D semiconductor monolayers and reassembly of organic/inorganic artificial superlattices. *Chem* **7**, 1887-1902, doi:https://doi.org/10.1016/j.chempr.2021.03.022 (2021).
190 Gibertini, M., Koperski, M., Morpurgo, A. F. & Novoselov, K. S. Magnetic 2D materials and heterostructures. *Nat Nanotechnol* **14**, 408-419, doi:10.1038/s41565-019-0438-6 (2019).
191 Cui, C., Xue, F., Hu, W.-J. & Li, L.-J. Two-dimensional materials with piezoelectric and ferroelectric functionalities. *npj 2D Materials and Applications* **2**, 18, doi:10.1038/s41699-018-0063-5 (2018).
192 Hossain, M. *et al.* Recent Advances in Two-Dimensional Materials with Charge Density Waves: Synthesis, Characterization and Applications. *Crystals* **7**, 298 (2017).

193 Zomer, P. J., Dash, S. P., Tombros, N. & Wees, B. J. v. A transfer technique for high mobility graphene devices on commercially available hexagonal boron nitride. *Applied Physics Letters* **99**, 232104, doi:10.1063/1.3665405 (2011).
194 Schneider, G. F., Calado, V. E., Zandbergen, H., Vandersypen, L. M. K. & Dekker, C. Wedging Transfer of Nanostructures. *Nano Lett* **10**, 1912-1916, doi:10.1021/nl1008037 (2010).
195 Yang, R., Zheng, X., Wang, Z., Miller, C. J. & Feng, P. X.-L. Multilayer MoS2 transistors enabled by a facile dry-transfer technique and thermal annealing. *Journal of Vacuum Science & Technology B* **32**, 061203, doi:10.1116/1.4898117 (2014).
196 Zomer, P. J., Guimarães, M. H. D., Brant, J. C., Tombros, N. & Wees, B. J. v. Fast pick up technique for high quality heterostructures of bilayer graphene and hexagonal boron nitride. *Applied Physics Letters* **105**, 013101, doi:10.1063/1.4886096 (2014).
197 Pizzocchero, F. *et al.* The hot pick-up technique for batch assembly of van der Waals heterostructures. *Nat Commun* **7**, 11894, doi:10.1038/ncomms11894 (2016).
198 Son, S. *et al.* Strongly adhesive dry transfer technique for van der Waals heterostructure. *2D Mater* **7**, 041005, doi:10.1088/2053-1583/abad0b (2020).

Highlighted References

13 Novoselov, K. S. et al. Electric field effect in atomically thin carbon films. Science **306**, 666-669, doi:10.1126/science.1102896 (2004).

The first report of the exfoliation of single-layer graphene using adhesive tape.

21 Radisavljevic, B., Radenovic, A., Brivio, J., Giacometti, V. & Kis, A. Single-layer MoS2 transistors. Nat Nanotechnol **6**, 147-150, doi:10.1038/Nnano.2010.279 (2011).

First demonstration of a transistor from a monolayer semiconductor (MoS_2), prepared by mechanical exfoliation from a layered bulk crystal.

27 Huang, Y. et al. Reliable Exfoliation of Large-Area High-Quality Flakes of Graphene and Other Two-Dimensional Materials. ACS Nano **9**, 10612-10620, doi:10.1021/acsnano.5b04258 (2015).

This paper reported an oxygen plasma enhanced exfoliation method, which can produce large-area 2D crystals including graphene and the high-temperature superconductor bismuth strontium calcium copper oxide (Bi-2212).

33 Huang, Y. et al. Universal mechanical exfoliation of large-area 2D crystals. Nat Commun **11**, 2453, doi:10.1038/s41467-020-16266-w (2020).

This paper introduced a universal mechanical exfoliation technology for large-area 2D crystals that uses Au films to enhance the interfacial interaction between a 2D material and a substrate.

36 Frisenda, R. et al. Recent progress in the assembly of nanodevices and van der Waals heterostructures by deterministic placement of 2D materials. Chemical Society Reviews **47**, 53-68, doi:10.1039/C7CS00556C (2018).

This tutorial review reported all the details information about deterministic transfer methods. The information was compiled and shared in a pedagogical way and differences, advantages and challenges of the different deterministic transfer methods were presented.

41 Castellanos-Gomez, A. et al. Deterministic transfer of two-dimensional materials by all-dry viscoelastic stamping. 2D Mater **1**, 011002, doi:10.1088/2053-1583/1/1/011002 (2014).

This work presented an all-dry alternative to the wet-based deterministic transfer methods reported to that day, including all the technical details to allow other labs to easily replicate the technique, information that was somewhat missing in the articles reporting other deterministic transfer methods.

52 Sahoo, P. K., Memaran, S., Xin, Y., Balicas, L. & Gutierrez, H. R. One-pot growth of two-dimensional lateral heterostructures via sequential edge-epitaxy. *Nature* **553**, 63-67 (2018).

This paper introduces the water-assisted one-pot CVD method for growth of 2D multi-junction heterostructures.

58 Xie, S. E. *et al.* Coherent, atomically thin transition-metal dichalcogenide superlattices with engineered strain. *Science* **359**, 1131-1135, doi:10.1126/science.aao5360 (2018).

This paper describes the modulated MOCVD approach for producing 2D lateral superlattices.

59 Zhang, Z. W. *et al.* Robust epitaxial growth of two-dimensional heterostructures, multiheterostructures, and superlattices. *Science* **357**, 788-792, doi:DOI 10.1126/science.aan6814 (2017).

This paper introduces the multi-steps CVD approach for lateral 2D heterostructures with reverse flow capability for better control of sample quality.

65 Sun, L. *et al.* Chemical vapour deposition. *Nat Rev Methods Primers* **1**, 5, doi:https://doi.org/10.1038/s43586-020-00005-y (2021).

This review describes the basics of the CVD technique, its different components, procedures, as well as materials characterization techniques.

71 Li, J. *et al.* General synthesis of two-dimensional van der Waals heterostructure arrays. *Nature* **579**, 368-374, doi:10.1038/s41586-020-2098-y (2020).

This work reported the scalable synthesis of 2D van der Waals heterostructure arrays on existing 2D semiconductors.

81 Sutter, P., Wang, J. & Sutter, E. Wrap-Around Core–Shell Heterostructures of Layered Crystals. *Adv Mater* **31**, 1902166, doi:https://doi.org/10.1002/adma.201902166 (2019).

This paper introduced a new type of van der Waals heterostructure with promising light harvesting properties, opening up van der Waals architectures beyond the archetypal vertical stacks and laterally stitched 2D layers.

87 Sutter, P., Khorashad, L. K., Argyropoulos, C. & Sutter, E. Cathodoluminescence of Ultrathin Twisted $Ge_{1-x}Sn_xS$ van der Waals Nanoribbon Waveguides. *Adv Mater* **33**, 2006649, doi:https://doi.org/10.1002/adma.202006649 (2021).
This paper discusses synthetic ultrathin 3D-shaped van der Waals nanoribbon waveguides and explains the coherent electron-beam excitation of photonic modes in such waveguides.

96 Cao, Y. *et al.* Correlated insulator behaviour at half-filling in magic-angle graphene superlattices. *Nature* **556**, 80-84, doi:10.1038/nature26154 (2018).
This paper reported the first experimental observation of gate-tunable electron correlation effects due to flat bands in magic-angle twisted bilayer graphene.

98 Zhao, Y. et al. Supertwisted spirals of layered materials enabled by growth on non-Euclidean surfaces. Science **370**, 442-445, doi:doi:10.1126/science.abc4284 (2020).
This work demonstrated control over interlayer twist in dislocated growth spirals of transition metal dichalcogenides synthesized on non-planar substrates.

105 Sutter, P., Wimer, S. & Sutter, E. Chiral twisted van der Waals nanowires. *Nature* **570**, 354-357, doi:10.1038/s41586-019-1147-x (2019).
This study showed that Eshelby twist in van der Waals nanowires gives rise to precisely tunable interlayer twist and demonstrated modulated optoelectronic properties due to changing interlayer moiré registries in single nanowires.

147 Liu, Y. *et al.* Approaching the Schottky–Mott limit in van der Waals metal–semiconductor junctions. *Nature* **557**, 696-700, doi:10.1038/s41586-018-0129-8 (2018).
This study generalized van der Waals integration of 3D metal thin-film electrodes with 2D semiconductors to create nearly ideal metal–semiconductor junctions.

149 Liao, L. *et al.* High-κ oxide nanoribbons as gate dielectrics for high mobility top-gated graphene transistors. *Proceedings of the National Academy of Sciences* **107**, 6711-6715, doi:10.1073/pnas.0914117107 (2010).
This study first demonstrated damage-free 2D semiconductor–dielectric van der Waals integration with a pristine interfaces and retained electronic performance.

194 Zhao, B. *et al.* High-order superlattices by rolling up van der Waals heterostructures. *Nature* **591**, 385-390, doi:10.1038/s41586-021-03338-0 (2021).
This study first demonstrated a series of high-order vdW superlattices that are difficult to achieve using exfoliation and restacking approaches.

Acknowledgements

P.S. and E.S. acknowledge support from the National Science Foundation, Division of Materials Research, Solid State and Materials Chemistry Program under Grant No. DMR-1607795 (twisted nanowire synthesis and diffraction analysis), the Department of the Navy, Office of Naval Research under ONR Award No. N00014-20-1-2305 (twisted nanowire optoelectronics), and the U.S. Department of Energy, Office of Science, Basic Energy Sciences, under Award No. DE-SC0016343 (synthesis of twisted stacks, development of STEM-CL spectroscopy).

J.Q. acknowledges financial support from the Agencia Estatal de Investigación of Spain (Grant PID2019-106820RB) and from Universidad Complutense de Madrid and European Commision (MSCA COFUND UNA4CAREER grant. Project number 4129252). A.C.G. acknowledges funding from the European Research Council (ERC) under the European Union's Horizon 2020 research and innovation program (Grant Agreement No. 755655, ERC-StG 2017 project 2D-TOPSENSE), the EU FLAG-ERA project To2Dox (JTC-2019-009), the Comunidad de Madrid through the CAIRO-CM project (Y2020/NMT-6661) and the Spanish Ministry of Science and Innovation (grant PID2020-118078RB-I00).

Y.H. acknowledges support from the National Key Research and Development Program of China (Grant No. 2019YFA0308000, 2018YFA0704201), the National Natural Science Foundation of China (NNSFC, Grant No. 62022089, 11874405), Chongqing Outstanding Youth Fund (grant No. 2021ZX0400005) and the Strategic Priority Research Program (B) of the Chinese Academy of Sciences (Grant No. XDB30000000).

X.D. acknowledges financial support by the Office of Naval Research through grant number N00014-18-1-2707.

H.R.G. acknowledges support by the National Science Foundation grant DMR-1557434.

Z.F. is supported by the National Science Foundation under Grant No. DMR-1945560

Author contributions

Introduction (P.S.); Experimentation (A.C.G., H.G., Y.H., X.H., J.Q., E.S. and P.S.); Results (H.G., E.S., and P.S.); Applications (A.C.G., X.D., Z.F., Y.H., X.H., J.Q., Q.Q., E.S. and P.S.); Reproducibility and data deposition (A.C.G., H.G., J.Q., and P.S.); Limitations and optimizations (A.C.G., H.G., J.Q., and P.S.); Outlook (A.C.G., X.D., H.G., J.Q., E.S. and P.S.).

Competing Interests

The authors declare no competing interests.